Tripathi V, Ellis JD, Shen Z, Song DY, Pan Q, Watt AT, Freier SM, Bennett CF, Sharma A, Bubulya PA, Blencowe BJ, Prasanth SG, Prasanth KV (2010) The nuclear-retained noncoding RNA MALAT1 regulates alternative splicing by modulating SR splicing factor phosphorylation. Mol Cell 39:925–938

Ule J, Jensen KB, Ruggiu M, Mele A, Ule A, Darnell RB (2003) CLIP identifies Nova-regulated RNA networks in the brain. Science 302: 1212–1215

Ule J, Ule A, Spencer J, Williams A, Hu JS, Cline M, Wang H, Clark T, Fraser C, Ruggiu M, Zeeberg BR, Kane D, Weinstein JN, Blume J, Darnell RB (2005) Nova regulates brain-specific splicing to shape the synapse. Nat Genet 37:844–852

Wang ET, Cody NA, Jog S, Biancolella M, Wang TT, Treacy DJ, Luo S, Schroth GP, Housman DE, Reddy S, Lecuyer E, Burge CB (2012) Transcriptome-wide regulation of pre-mRNA splicing and mRNA localization by muscleblind proteins. Cell 150:710–724

Xue Y, Zhou Y, Wu T, Zhu T, Ji X, Kwon YS, Zhang C, Yeo G, Black DL, Sun H, Fu XD, Zhang Y (2009) Genome-wide analysis of PTB-RNA interactions reveals a strategy used by the general splicing repressor to modulate exon inclusion or skipping. Mol Cell 36:996–1006

Yano M, Okano HJ, Okano H (2005) Involvement of Hu and heterogeneous nuclear ribonucleoprotein K in neuronal differentiation through p21 mRNA post-transcriptional regulation. J Biol Chem 280:12690–12699

Yano M, Hayakawa-Yano Y, Mele A, Darnell RB (2010) Nova2 regulates neuronal migration through an RNA switch in disabled-1 signaling. Neuron 66:848–858

Yeo GW, Coufal NG, Liang TY, Peng GE, Fu XD, Gage FH (2009) An RNA code for the FOX2 splicing regulator revealed by mapping RNA-protein interactions in stem cells. Nat Struct Mol Biol 16:130–137

Zhang C, Darnell RB (2011) Mapping in vivo protein-RNA interactions at single-nucleotide resolution from HITS-CLIP data. Nat Biotechnol 29:607–614

Zhang YQ, Bailey AM, Matthies HJ, Renden RB, Smith MA, Speese SD, Rubin GM, Broadie K (2001) Drosophila fragile X-related gene regulates the MAP1B homolog Futsch to control synaptic structure and function. Cell 107:591–603

Zhang C, Frias MA, Mele A, Ruggiu M, Eom T, Marney CB, Wang H, Licatalosi DD, Fak JJ, Darnell RB (2010) Integrative modeling defines the Nova splicing-regulatory network and its combinatorial controls. Science 329:439–443

Zheng S, Gray EE, Chawla G, Porse BT, O'ell TJ, Black DL (2012) PSD-95 is post-transcriptionally repressed during early neural development by PTBP1 and PTBP2. Nat Neurosci 15(381–8):S1

Zhong XY, Wang P, Han J, Rosenfeld MG, Fu XD (2009) SR proteins in vertical integration of gene expression from transcription to RNA processing to translation. Mol Cell 35:1–10

Journal of Neuroscience Research

Journal of Neuroscience Research 93:399–409 (2015)

Alternative Role of HuD Splicing Variants in Neuronal Differentiation

Satoru Hayashi,[1,2] Masato Yano,[1] Mana Igarashi,[1] Hirotaka James Okano,[1,3] and Hideyuki Okano[1]*

[1]Department of Physiology, Keio University School of Medicine, Tokyo, Japan
[2]CNS Drug Discovery Unit, Pharmaceutical Research Division, Takeda Pharmaceutical Company Limited, Kanagawa, Japan
[3]Division of Regenerative Medicine, Jikei University School of Medicine, Tokyo, Japan

HuD is a neuronal RNA-binding protein that plays an important role in neuronal differentiation of the nervous system. HuD has been reported to have three RNA recognition motifs (RRMs) and three splice variants (SVs) that differ in their amino acid sequences between RRM2 and RRM3. This study investigates whether these SVs have specific roles in neuronal differentiation. In primary neural epithelial cells under differentiating conditions, HuD splice variant 1 (HuD-sv1), which is a general form, and HuD-sv2 were expressed at all tested times, whereas HuD-sv4 was transiently expressed at the beginning of differentiation, indicating that HuD-sv4 might play a role compared different from that of HuD-sv1. Indeed, HuD-sv4 did not promote neuronal differentiation in epithelial cells, whereas HuD-sv1 did promote neuronal differentiation. HuD-sv4 overexpression showed less neurite-inducing activity than HuD-sv1 in mouse neuroblastoma N1E-115 cells; however, HuD-sv4 showed stronger growth-arresting activity. HuD-sv1 was localized only in the cytoplasm, whereas HuD-sv4 was localized in both the cytoplasm and the nuclei. The Hu protein has been reported to be involved in translation and alternative splicing in the cytoplasm and nuclei, respectively. Consistent with this observation, HuD-sv1 showed translational activity on p21, which plays a role in growth arrest and neuronal differentiation, whereas HuD-sv4 did not. By contrast, HuD-sv4 showed stronger pre-mRNA splicing activity than did HuD-sv1 on Clasp2, which participates in cell division. Therefore, HuD SVs might play a role in controlling the timing of proliferation/differentiation switching by controlling the translation and alternative splicing of target genes.

Key words: HuD (ELAVL4); development; RNA splicing

Recent studies have revealed that posttranscriptional regulation plays an important role in cell differentiation and development by controlling gene translation (Ostareck et al., 1997; Imai et al., 2001; Okabe et al., 2001; Okano et al., 2002). One advantage of controlling genes at the posttranscriptional level is that it allows rapid changes in gene expression without de novo mRNA synthesis. Thus, posttranscriptional regulation allows precise control of timing during rapidly progressing biological events, such as development. The molecules determining mRNA posttranscriptional regulation include RNA-binding proteins that specifically recognize *cis*-elements in mRNA sequences (Darnell, 2002).

Hu proteins, which were first identified as target antigens in a paraneoplastic neurological syndrome (Hu syndrome), consist of four subtypes: HuA (HuR, Elavl1), HuB (Hel-N1, Elavl2), HuC (Ple-21, Elavl3), and HuD (Elavl4; Szabo et al., 1991; Dalmau et al., 1992; Good, 1995, 1997). These four subtypes have been cloned (Szabo et al., 1991; Levine et al., 1993; Sakai et al., 1994; Ma et al., 1996) and identified as RNA-binding proteins similar to the *Drosophila* Elav protein, which is required for the differentiation and survival of neurons (Homyk et al., 1985; Robinow et al., 1988). HuB, HuC, and HuD are expressed in both early postmitotic and mature neurons, and HuA is expressed ubiquitously (Okano and Darnell, 1997; Ma et al., 1996). Neuron-type Hu also plays an important role in mammalian neuronal differentiation (Akamatsu et al., 1999; Kasashima et al., 1999). Hu proteins contain three well-characterized RNA recognition motifs (RRMs) that mediate specific and high-affinity binding to GU-rich sequences and to AU-rich elements of target mRNAs (Fan and Steitz, 1998; Ince-Dunn et al., 2012). The RNA-binding ability of the

This article was published online on 21 October 2014. An error was subsequently identified. This notice is included in the online and print versions to indicate that both have been corrected on 31 October 2014.

Contract grant sponsor: Ministry of Education, Culture, Sports, Science, and Technology Leading Project for Realization of Regenerative Medicine of Japan (to H.O.); Contract grant sponsor: Japanese Ministry of Health, Labour, and Welfare Research Grant on Measures for Intractable Diseases (to H.O.); Contract grant sponsor: Grants-in-Aid for Scientific Research on Innovative Areas; Contract grant number: 24111543 (to H.J.O.).

*Correspondence to: Hideyuki Okano, 35 Shinanomachi, Shinjuku-ku, Tokyo 160–8582, Japan. E-mail: hidokano@a2.keio.jp

Received 14 July 2014; Revised 26 August 2014; Accepted 18 September 2014

Published online 21 October 2014 in Wiley Online Library (wileyonlinelibrary.com). DOI: 10.1002/jnr.23496

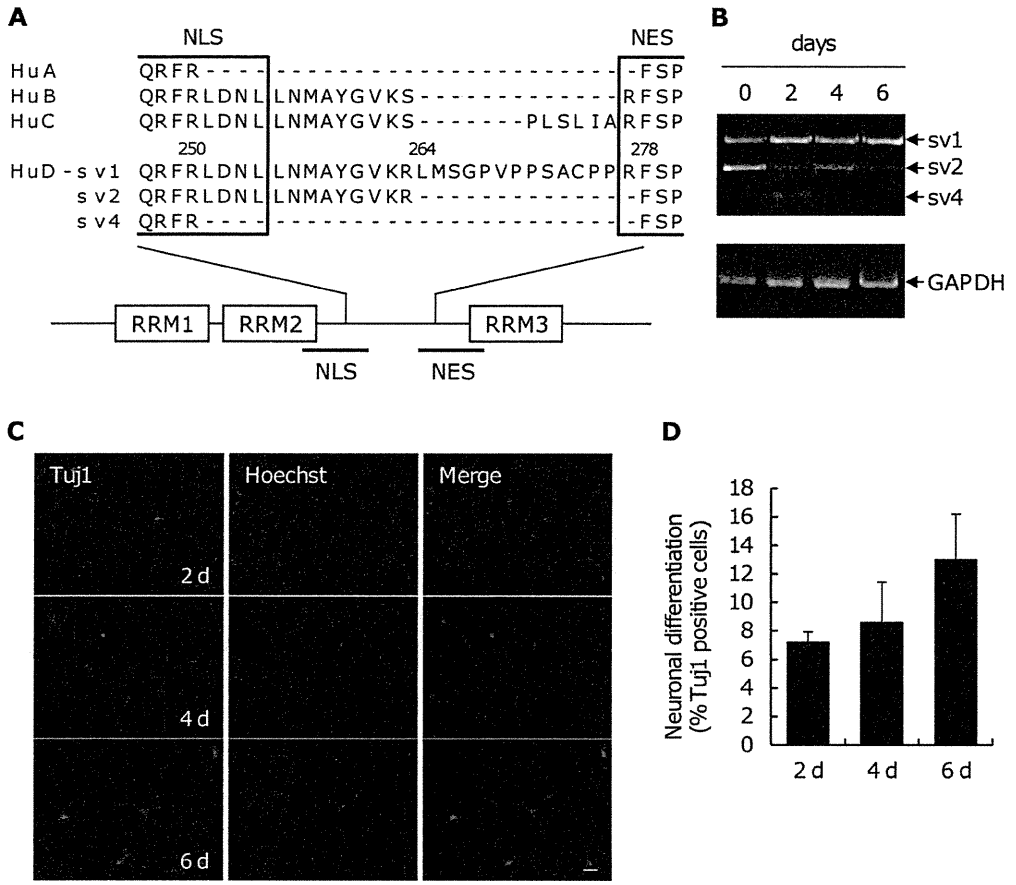

Fig. 1. HuD-sv4 was expressed only in the early phase of neuronal differentiation in neural epithelial cells. **A:** Schematic structure of HuD. HuD has three SVs between RRM2 and RRM3, with a partially overlapping NLS and NES. The amino acid sequences are shown in single-letter code with gaps as hyphens. **B:** RT-PCR analysis of differentiating neural epithelial cells. Neural epithelial cells were prepared from embryonic-day 14 mice as described in Materials and Methods. Cultivated cells were replated at 4 days in vitro and incubated for another 2, 4, and 6 days under differentiation conditions. Then, the expression levels of HuD SVs were detected by RT-PCR analysis. Glyceraldehyde-3-phosphate dehydrogenase mRNA expression was used as an internal control for each sample. **C:** Induction of neuronal differentiation from neural epithelial cells by cultivating differentiation-inducing medium. The cells were cultivated as described for B and immunostained for βIII-tubulin. **D:** Quantification results of C. The ratios of βIII-tubulin-positive cells to Hoechst-positive cells are shown as mean ± SD. Scale bar = 200 μm.

RRM1 and RRM2 domains is required for Hu proteins to induce neurite extension in PC12 cells (Akamatsu et al., 1999). Moreover, Hu proteins have been shown to regulate the stability and/or the translation of several putative target mRNAs encoding proteins that play important roles in the regulation of differentiation and proliferation (Chung et al., 1997; Gorospe et al., 1998; Joseph et al., 1998; Antic et al., 1999; Aranda-Abreu et al., 1999; Tenenbaum et al., 2000; Wang et al., 2000; Kullmann et al., 2002). These findings suggest that the simultaneous regulation of the expression of these mRNAs by neuronal Hu might play an important role in controlling the timing of growth/differentiation switching. At the time when those studies were performed, splice variants (SVs) were not considered. However, we reported that HuD has three SVs, HuD-sv1, HuD-sv2, and HuD-sv4, in the spacer region between RRM2 and RRM3 (Okano and Darnell, 1997; Fig. 1A). The longest form (HuD-sv1), which is the general form, is considered to play roles in neural differentiation, as mentioned above (Homyk et al., 1985; Robinow et al., 1988; Okano and Darnell, 1997; Fan and Steitz, 1998; Akamatsu et al., 1999; Kasashima et al., 1999). However, the functions of other HuD SVs remain unclear. The HuD nuclear localization signal (NLS) and HuD nuclear export signal (NES) between RRM2 and RRM3 might be important for inducing neuronal differentiation by HuD (Kasashima et al., 1999). HuD-sv2 and -sv4 lack a portion of the NLS or NES. These findings suggest that the SVs of HuD can present variable localization patterns in cells and play different roles in neuronal differentiation.

In this study, the neuronal differentiation and cell-growth-arresting activities of the HuD SVs are examined and compared with HuD-sv1. These activities are principal functions of neuronal Hu and are important for neuronal development regulation by Hu.

MATERIALS AND METHODS

Animal Experiment

This study was approved and carried out in accordance with the guidelines of the Institutional Animal Care and Use Committee of Keio University. All efforts were made to minimize animal suffering.

Plasmid Construction

The pCXN2 vector, which carries a CAG promoter, was a kind gift from Dr. H. Niwa (Niwa et al., 1991). The HuD SV cDNAs were cloned from a cDNA library of mouse brain by reverse transcription-polymerase chain reaction (RT-PCR), and their sequences were confirmed. Each obtained clone was inserted into the pGEM-myc vector, which is a pGEM vector (Promega, Madison, WI) carrying a myc-tag sequence upstream of multiple cloning sites. Then, the *NotI*-cleaved segments were inserted into pCXN2.

Preparation of HuD-Carrying Lentivirus

The HuD cDNAs with the myc-tag sequence at the 5′ terminus were subcloned into the pCSII-EF-MCS-IRES2-Venus vector, which was modified to include the EF promoter as the expression promoter and which possesses an automatic expression fluorescent protein (Venus) system based on IRES (Miyoshi et al., 1998; Nagai et al., 2002). Dissociated 293T cells (ATCC, Manassas, VA) were seeded into T-175 culture flasks at a density of 1×10^7 cells/flask. The cells were incubated for 24 hr at 37°C in a humidified incubator with an atmosphere of 5% CO_2. The pCSII-EF-MSC-IRES2-Venus carrying HuD, pMDLg/pRRE, pRSV-Rev, and pcDNA3.1-VSV-G vectors was transfected into the cells with FreeStyle 293 medium (Invitrogen, Carlsbad, CA) and FuGENE6 (Roche Diagnostics, Mannheim, Germany) according to the manufacturers' protocols. After incubation for 12–16 hr, the medium was exchanged for proliferation medium. After a further incubation for 56–60 hr, the supernatant was collected and passed through 0.45-μm cassette filters. The virus-containing solution was centrifuged at 50,000*g* for 2 hr at 4°C, and the precipitate containing virus particles was dried for 5 min. After phosphate-buffered saline (PBS) had been added to the virus particles, these particles were incubated overnight at 4°C. The virus solution was thoroughly resuspended by pipetting and stored at −80°C until use. Virus titration was determined by fluorescence-activated cell sorting with Venus fluorescence. Epithelial cells were infected with virus at a multiplicity of infection (MOI) of 0.5.

Preparation of Mouse Epithelial Cells

The brains were collected from ICR mice at embryonic day 14 (Japan SLC, Shizuoka, Japan). The cerebral cortex was separated and added to multipurpose handling medium (MHM), which consisted of Dulbecco's modified Eagle's medium (DMEM)/F12 (Invitrogen) supplemented with 25 μg/ml insulin (Sigma, St. Louis, MO), 100 μg/ml apotransferrin (Sigma), 20 nmol/liter progesterone (Sigma), 100 μmol/liter putrescine (Sigma), 30 nmol/liter sodium selenite (Sigma), and 10 ng/ml basic fibroblast growth factor (bFGF; R&D Systems, Minneapolis, MN). The cerebral cortex was dissociated by pipetting and centrifuged at 900*g* for 3 min at room temperature. The collected cells were suspended in fresh MHM and seeded onto polyornithine/fibronectin-coated culture dishes (two or three embryos/10-cm dish). After 1 day, bFGF was added to a final concentration of 5 ng/ml. On the next day, the entire volume of medium was removed and fresh MHM was added. After incubation for 1 additional day, bFGF was added to a final concentration of 5 ng/ml. At 4 days after plating, the cells were dissociated from the culture dish by pipetting, and the number of collected cells was determined. The cells were resuspended in MHM or in MHM without bFGF (differentiation-inducing medium) and seeded onto polyornithine/fibronectin-coated 24-well plates at a density of 8×10^4 cells/well. After 24 hr of incubation, the lentiviruses carrying each HuD SV were added. The cells were cultivated for 6 days and subjected to immunocytochemical analysis.

RT-PCR Analysis of Epithelial Cells

Total RNA isolation and first-strand cDNA synthesis were performed with an RNeasy Mini kit (Qiagen, Hilden, Germany) and a cDNA reverse transcription kit (Applied Biosystems, Foster City, CA), respectively, following the manufacturers' protocols. PCR was performed with specific HuD primers (5′-TTACTG TGAAGTTTGCCA-3′, 5′-GATGTTCATTCCCACAAG-3′) surrounding the coding region of RRM2 and RRM3. Band intensities were quantified in ImageJ.

Neurite Outgrowth and Cell-Growth Assay

N1E-115 cells (ATCC) were cultured in 24-well plates, and each myc-tagged HuD SV (0.5 μg) was cotransfected with pCXN2-monomeric red fluorescent protein (mRFP) expression vector (0.1 μg) with FuGENE6 reagents. pCXN2-mRFP was used as a marker of transfected cells. In the neurite outgrowth assay, three or four random photographs/well were taken at 4 days after transfection. Then, the cells that were both mRFP positive and extending neurites longer than the cell diameter were counted. The data are presented as the ratio of the number of neurite-bearing cells to the total number of mRFP-positive cells (more than 100 cells were counted). In the cell-growth assay, mRFP-positive cells were counted at days 1 and 3, and the relative cell growth from day 1 to day 3 was calculated.

Immunocytochemical Analysis

HuD SV-transfected cells were fixed in PBS containing 4% paraformaldehyde for 15 min at room temperature. After fixation, the cells were permeabilized by 0.3% Tween-20 in PBS and incubated in TBA blocking reagent (Roche Diagnostics) for 30 min at room temperature. Then, the cells were incubated with an anti-βIII-tubulin antibody (1:1,000 dilution; mouse monoclonal IgG; Sigma), an anti-myc antibody (1:1,000 dilution; mouse monoclonal IgG; Sigma), or an anti-green fluorescent protein antibody (1:1,000 dilution; mouse monoclonal

IgG; a gift from Dr. S. Mitani, Tokyo Women's Medical University School of Medicine) in TBA blocking reagent overnight at 4°C. The cells were washed three times in PBS and incubated with the appropriate secondary antibodies Alexa Fluor 488 goat anti-mouse IgG or Alexa Fluor 568 goat anti-mouse IgG (Invitrogen) and Hoechst 33342 (Invitrogen) for 1 hr at room temperature. Fluorescent signals were detected with an ApoTome attachment (Carl Zeiss, Jena, Germany).

Cell Fractionation and Immunoblotting Analysis

N1E-115 cells were transfected with the HuD SVs. After they had been incubated for 2 days, the cells were collected into a tube, and buffer A, consisting of 10 mmol/liter HEPES-KOH (pH 7.8), 10 mmol/liter KCl, 0.1 mmol/liter EDTA (pH 8.0), 0.1% NP-40, and protease inhibitor cocktail (Roche Diagnostics), was added. The cell suspension was vortexed well and centrifuged at 2,300*g* for 1 min at 4°C to obtain the supernatant as a cytoplasmic fraction. Buffer B, consisting of 50 mmol/liter HEPES-KOH (pH 7.8), 420 mmol/liter KCl, 0.1 mmol/liter EDTA (pH 8.0), 5 mmol/liter $MgCl_2$, 2% glycerol, and protease inhibitor cocktail, was added to the precipitate. Then, the sample was placed on ice for 30 min and centrifuged at 20,400*g* for 15 min at 4°C. The supernatant was collected as a nucleic fraction. The collected fractions were separated with sodium dodecyl sulfate-polyacrylamide electrophoresis and electrically transferred to an Immobilon-P membrane (Millipore, Billerica, MA). The membranes were incubated in TBA blocking reagent for 30 min at room temperature and then incubated with an anti-myc monoclonal antibody (1:1,000 dilution; Sigma), anti-α-tubulin monoclonal antibody (Sigma), or antilamin monoclonal antibody (Cell Signaling Technology, Danvers, MA) for 2 hr at room temperature. After they had been washed three times in TBS, the membranes were incubated with an HRP-conjugated secondary antibody (Invitrogen). The membranes were then washed, and the blots were detected by enhanced chemiluminescense (Pierce, Rockford, IL).

Luciferase Reporter Assay

293T cells were cultured in 12-well plates and were transfected with a *Renilla* luciferase construct with or without p21 mRNA 3′-UTR, together with the pCXN2-HuD-sv1 or pCXN2-HuD-sv4 expression vector with FuGENE 6 reagent or Lipofectamine2000 (Invitrogen). The firefly luciferase expression vector was cotransfected as an internal control. The total amount of transfected DNA was equalized with the control pCXN2 vector. Transfected cells were cultivated for 2 days, and the luciferase activities were measured according to the recommended procedures for the dual luciferase assay system (Promega). A Lumat LB9507 luminometer (Berthold Technologies, Bad Wildbad, Germany) was used for luciferase detection. Transfected and cultivated cells were also subjected to RT-PCR analysis, which detects *Renilla* luciferase reporter gene by using specific primers (5′-TGCCTACCTGGAGCCA TTCAAG-3′, 5′-TTGCGGACAATCTGGACGAC-3′).

Splicing Reporter Assay

The pGlo containing the Clasp2 sequence was derived from pGloDab1.7bc (Yano et al., 2010), replacing the BamHI-EcoRI fragment from the mouse Clasp2 genome sequence, including exon 17 and exon 18, by PCR amplification. The primers used for cloning were 5′-AGGATCCAGTGGGTGTT GAGAGTAAAG-3′ and 5′-AGAATTCACATCGGAGCCT GTGTTTAG-3′. 293T cells were cultured in 96-well plates and were transfected with the reporter genes and HuD SVs. After 24 hr, mRNA was extracted by using an RNeasy 96 kit (Qiagen) and reverse transcribed by using MuLV reverse transcriptase (Applied Biosystems). Synthesized cDNA was amplified by PCR with Accuprime Supermix I (Invitrogen) and specific primers (5′-CTGAGGAGAAGTCTGCCGTTACTG-3′, 5′-AGAATTCACATCGGAGCCTGTGTTTAG-3′). PCR products were separated by 6% polyacrylamide gel electrophoresis and stained with SYBR Gold (Invitrogen). Band intensities were quantified in ImageJ.

Statistical Analyses

Statistical analyses were performed with Student's *t*-test, Welch's test, or Dunnett's test to compare the mean values of the control group and the tested groups.

RESULTS

HuD-sv1 but not HuD-sv4 Induced Neural Differentiation in Neural Epithelial Cells

We previously reported that HuD-sv1 and -sv2 were expressed during all stages of *in vivo* neural differentiation, whereas HuD-sv4 was expressed only during the early stage (Okano and Darnell, 1997). For the first step of evaluation *in vitro*, we investigated the timing of the expression of HuD SVs in primary neural epithelial cells containing neural stem cells. After induction of neuronal differentiation, the mRNA expression of the HuD SVs was detected by RT-PCR analysis. In agreement with a previous report, HuD-sv4 was also transiently expressed at day 2 *in vitro*, which accounted for 15% of HuD isoforms (Fig. 1B). This phase might be the early stage of neuronal differentiation in the cell because the percentage of cells positive for βIII-tubulin, which is a positive neuron marker, increased after 4 days (Fig. 1C,D; 6% of cells were βIII-tubulin positive at day 0 in an independent experiment). These results suggest that HuD-sv4 might have a role different from that of HuD-sv1 or -sv2. Next, the lentivirus carrying HuD-sv1 or -sv4 was constructed and infected into the neural epithelial cells under differentiating conditions at an MOI of 0.5. After 6 days, neural differentiation was evaluated by the ratio of βIII-tubulin-positive cells to infected cells (Venus-positive cells). For reasons that remain unclear, Venus-positive cells from HuD-sv4 infection were relatively fewer than those cells from control or HuD-sv1 infection. Under these conditions, the ratios of βIII-tubulin-positive cells in mock, HuD-sv1-infected, and HuD-sv4-infected cells were 23.0%, 41.5%, and 26.5%, respectively (Fig. 2).

Alternative Roles of HuD SVs in Neurite Outgrowth and Proliferation

We further investigated the function of HuD SVs with mouse neuroblastoma N1E-115 cells. N1E-115 cells

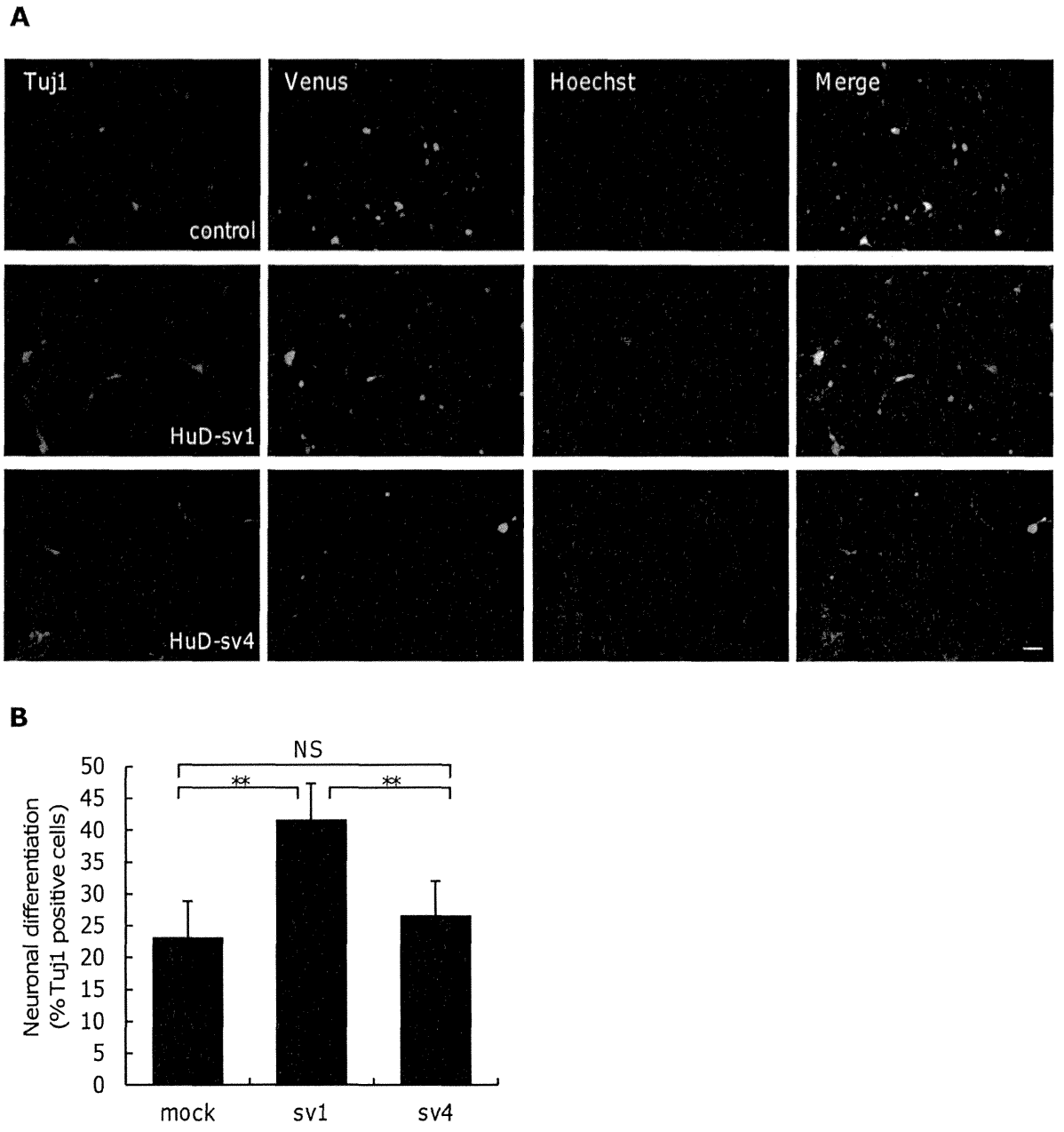

Fig. 2. HuD-sv1 but not HuD-sv4 induced neuronal differentiation in neural epithelial cells. Lentiviruses carrying each HuD SV were added under differentiating conditions at 1 day after replating. The cells were cultivated for another 6 days and immunostained by βIII-tubulin. Then, three random photographs/well were taken (**A**), and the ratios of βIII-tubulin-positive cells to Venus-positive (lentivirus infected) cells were quantified (**B**). The data are representative from four independent experiments. The values represent mean ± SD. $^{**}P < 0.01$, Student's *t*-test. NS, not significantly separated. Scale bar = 200 μm.

have the ability to arrest their cell cycle and to extend their neurites by introducing HuB (Yano et al., 2005). Therefore, the effect of HuD SVs on these cells could be evaluated, whereas neural epithelial cells did not proliferate enough to evaluate growth-arresting activities. N1E-115 cells were cotransfected with HuD-sv1, -sv2, or -sv4 together with mRFP. After 4 days of incubation, 25.4% of the cells exhibited neurite outgrowth in HuD-sv1 transfected cells (Fig. 3A), with a morphology similar to that of N1E-115 cells with HuB (data not shown). By contrast, HuD-sv2 and -sv4 showed less neurite outgrowth-induction activity than HuD-sv1 (21.4% and

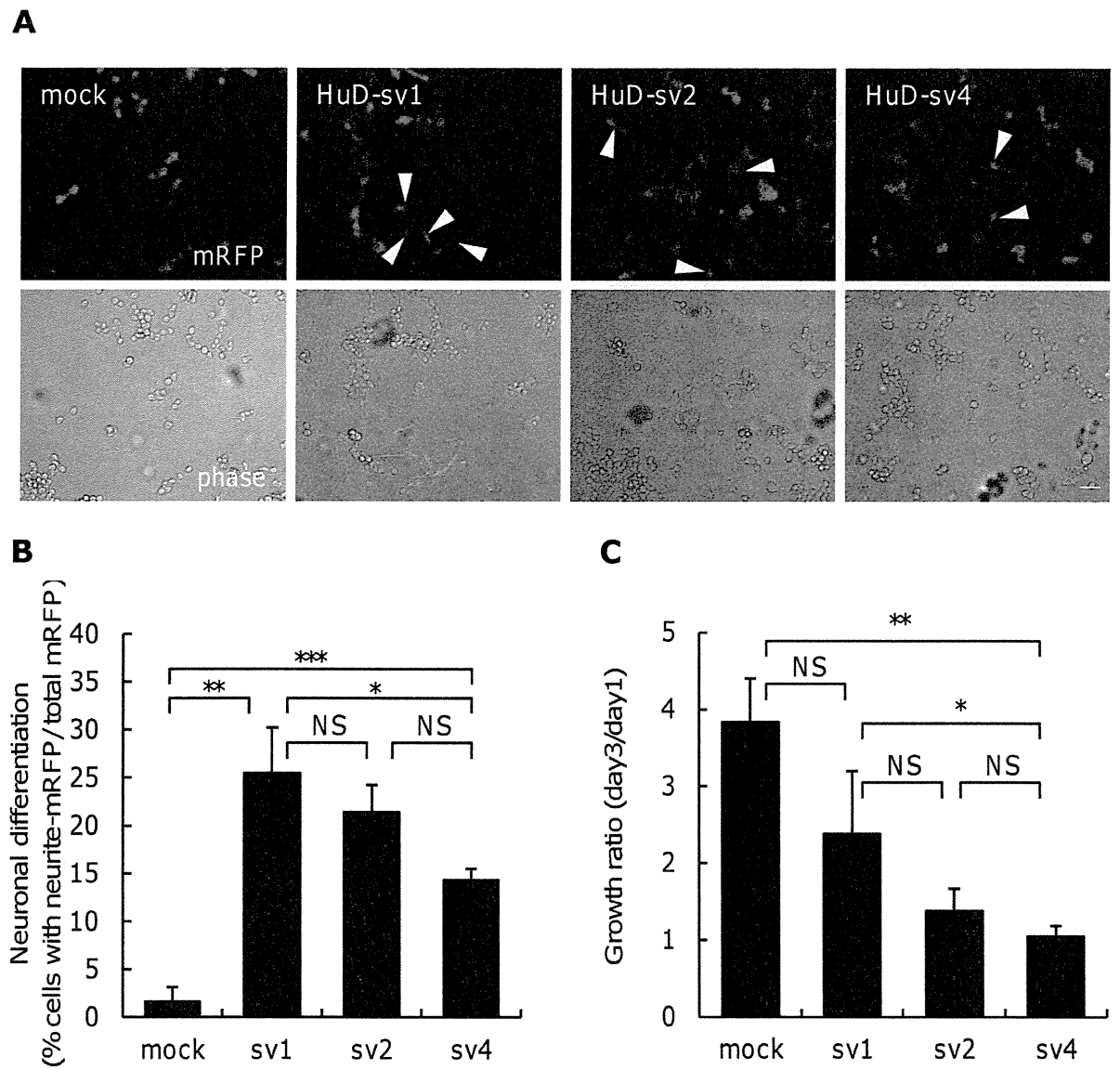

Fig. 3. Neurite induction and growth arrest by the HuD SVs in N1E-115 cells. **A:** Induction of neuronal differentiation by HuD overexpression. HuD SVs were transfected into N1E-115 cells with mRFP. Arrowheads indicate the neurite-bearing cells. **B:** Ratio of neurite-bearing cells in A was quantified as described in Materials and Methods. **C:** Growth arrest by HuD overexpression. mRFP was cotransfected into N1E-115 cells with HuD SVs, and the number of mRFP-positive cells was determined at days 1 and 3. The ratios of the numbers at day 3 to day 1 are shown. The values represent mean ± SD from more than three independent experiments. $*P < 0.05$, $**P < 0.01$, $***P < 0.001$, Student's *t*-test. NS, not significantly separated. Scale bar = 200 μm.

14.3%, respectively). The immunoblot analysis indicated that the expression level of each transfected SV was not altered (data not shown).

HuB elicits neuronal differentiation and cell cycle arrest by suppressing heterogeneous nuclear ribonucleoprotein K and the subsequent translation of the p21 protein (Yano et al., 2005). Therefore, we investigated the role of HuD SVs in cell-cycle regulation. After N1E-115 cells were cotransfected with mRFP and myc-HuD-sv1, -sv2, or -sv4, mRFP-positive cells were counted after 1 and 3 days. HuD-sv1 overexpression reduced the proliferation of N1E-115 cells to 2.4-fold compared with mock-transfected cells (3.8-fold; Fig. 3B). HuD-sv2 and -sv4 showed stronger negative proliferation regulation because the cell numbers increased 1.4 and 1.1-fold, respectively.

Intracellular Localization of HuD SVs

The distance between NLS and NES might be important in the nucleocytoplasmic shuttling of HuD and

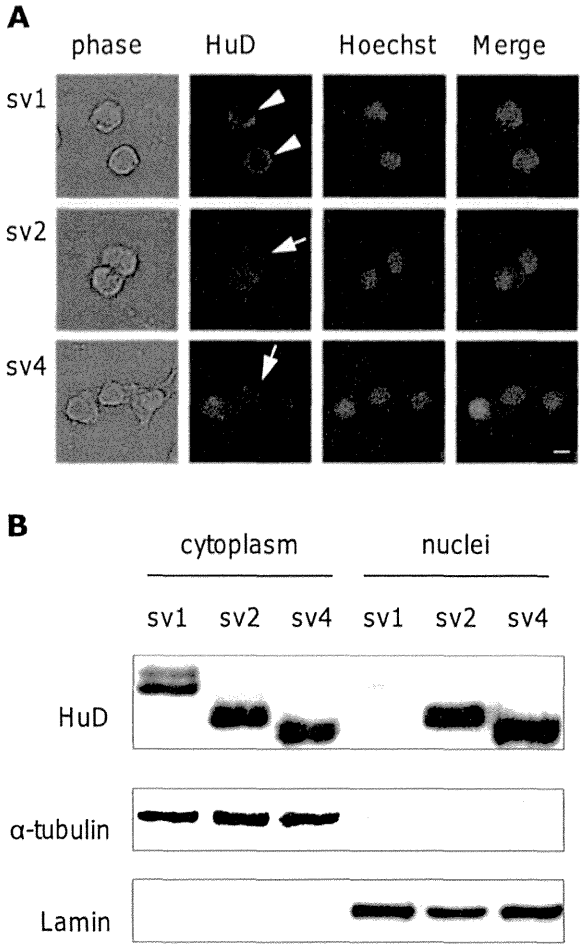

Fig. 4. Intracellular localization of myc-tagged HuD SVs. **A:** Immunocytochemical analysis of HuD-transfected cells. myc-Tagged HuD SVs were transfected into N1E-115 cells and immunostained by an anti-myc antibody after 2 days. Arrowheads indicate HuD that is almost localized in the cytoplasm, arrows in both the cytoplasm and the nuclei. **B:** Immunoblotting analysis of HuD-transfected cells. Cytoplasmic or nuclear fractions were prepared from the transfected cells and analyzed by Western blotting. α-Tubulin and lamin were used as markers of the cytoplasmic and nuclear fractions, respectively. Scale bar = 20 μm.

in the neurite induction activity in PC12 cells (Kasashima et al., 1999). Therefore, we investigated the intracellular localization of HuD SVs. N1E-115 cells were transfected with myc-HuD-sv1, -sv2, or -sv4 and cultivated for 2 days. Subsequent immunocytochemical analysis revealed that myc-HuD-sv1 was localized in the cytoplasm, whereas myc-HuD-sv2 or -sv4 existed in both the cytoplasm and the nuclei (Fig. 4A, see HuD column). To confirm the localization of HuD SVs, the cytoplasm and nuclei of the transfected cells were fractionated and subjected to immunoblotting analysis. As shown in Figure 4B, HuD SVs were localized to the portions that were observed in the immunocytochemical analysis, myc-HuD-sv1 was detected in the cytoplasmic fraction (positive for the cytoplasm marker α-tubulin), and myc-HuD-sv2 and -sv4 were detected in both cytoplasmic and nucleic fractions (positive for the nuclei marker lamin).

HuD-sv4 Has Weak Translational Activity on p21 mRNA

HuD targets numerous mRNAs and controls their translation. As can be observed in Figure 4, HuD-sv4 existed in both the cytoplasm and the nuclei, whereas HuD-sv1 localized in the cytoplasm. Note that mRNA translation occurs in the cytoplasm, so the translational activity of HuD-sv4 might be weaker than that of HuD-sv1. To test this hypothesis, a luciferase reporter assay, which was driven by the p21 mRNA 3′-UTR, was conducted. p21 mRNA is a well-known target of HuD, and HuD binding to the 3′-UTR stabilizes the mRNA and increases its translation (Joseph et al., 1998). We overexpressed luciferase reporters with each HuD SV in 293T cells, which are cells with high transfection efficiency that do not express HuB, HuC, or HuD, excluding the effects of endogenous Hu (data not shown). Luciferase activity was assayed as described in Materials and Methods. HuD-sv1 overexpression increased the relative reporter activity up to 178%, whereas HuD-sv4 overexpression increased the relative reporter activity up to 103% (Fig. 5A). HuD-sv1 and -sv4 did not change reporter mRNA level (Fig. 5B).

HuD-sv4 Shows Stronger Splicing Activity Than HuD-sv1

As mentioned above, HuD is an RNA-binding protein that regulates the translation of target genes. However, recent high-throughput sequencing of RNA isolated by UV cross-linking immunoprecipitation analyses showed that neuronal Hu binds intronic sequences and regulates alternative splicing of numerous genes in mice (Ince-Dunn et al., 2012). Taken together, these facts and the intracellular localization of HuD-sv4 in both nuclei and cytoplasm suggest that HuD-sv4 might play a role in alternative splicing, which occurred in nuclei. To examine this hypothesis, splicing reporters of Clasp2 and Dystonin were constructed (Fig. 6A). These genes have verified neuronal Hu-dependent alternative exons (Ince-Dunn et al., 2012); exon 17 of Clasp2 and exon 69 of Dystonin were included or excluded by alternative splicing. 293T cells were transfected with the splicing reporter gene and HuD SVs, and the SVs were evaluated by RT-PCR. In RFP-transfected or HuD-sv1-transfected cells, exon 17 of Clasp2 was removed by splicing, and a 165-nt band was observed (Fig. 6B,C). HuD-sv4 decreased Clasp2 mRNA lacking exon 17 to 0.3-fold and increased mRNA including exon 17 to 6.2-fold compared with RFP. By contrast, the entire exon 69 of Dystonin pre-mRNA was included in RFP-transfected cells (444 nt). HuD-sv1 (slightly) and HuD-sv4 (strongly) shifted exon 69, causing this exon to be skipped (resulting in 117 nt; HuD-sv1 and -sv4 included: 0.5-fold and 0.1-fold, skipped: 208-fold and 343-fold, respectively, compared with RFP; Fig. 6D,E). The total protein expression level was not different between HuD-sv1 and HuD-

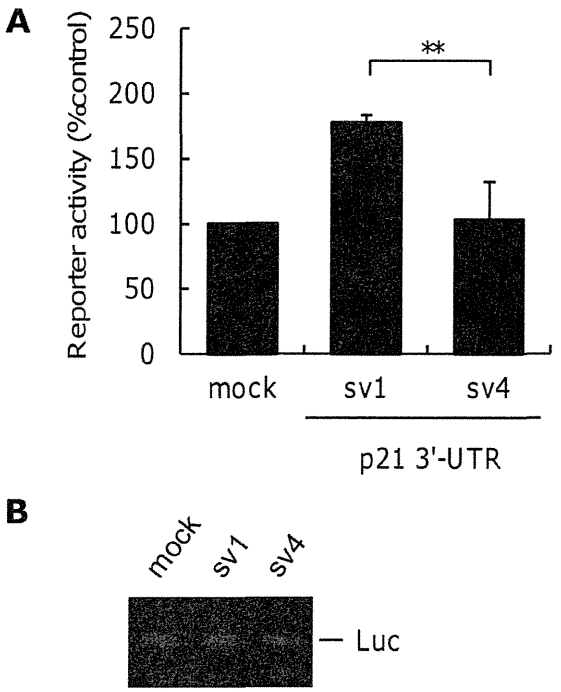

Fig. 5. Posttranscriptional control of p21 expression by HuD-sv1 and -sv4 in 293T cells. **A:** 293T cells were transfected with reporter constructs containing p21 mRNA 3′-UTR or with a control together with the HuD-sv1 or HuD-sv4 expression vector as described in Materials and Methods. Then, the cells were cultivated for 2 days and subjected to a luciferase activity assay. The values represent mean ± SD from five independent cultures. $^{**}P<0.01$, Welch's test. **B:** RT-PCR of reporter gene. 293T cells were transfected and cultivated as in A, and mRNA expression level of *Renilla* luciferase was analyzed by RT-PCR with specific primers.

sv4 and did not cause the difference in splicing activity (data not shown).

DISCUSSION

HuD SVs for Inducing Neuronal Differentiation and Growth Arrest

A recent genome-wide analysis indicated that over 90% of human genes undergo alternative splicing, which provides the primary means of protein diversity from a single gene (Blencowe, 2006; Wang et al., 2008). Although these genome-wide analyses found many newly spliced isoforms, they did not address the individual functions of these isoforms. The only way to reveal the functional differences between spliced variants is by a careful analysis with biochemical and biological methods. Our previous study indicated the existence of SVs in HuD; however, their physiological role remained to be elucidated. In this study, the roles of HuD SVs were analyzed *in vitro*. First, the expression patterns of the SVs were confirmed in neural epithelial cells, and HuD-sv4 was found to be transiently expressed during the early stage of neuronal differentiation, whereas HuD-sv1 and HuD-sv2 were expressed throughout the examined period. This finding was consistent with the embryonic expression of these variants *in vivo* (Okano and Darnell, 1997). The expression level of HuD-sv4 was no more than 15% of HuD SVs in the culture system; however, we consider that HuD-sv4 might play a characteristic role compared with HuD-sv1 and -sv2 because of its unique expression pattern. We subsequently found that HuD-sv4 overexpression induced neuronal differentiation extremely weakly in this culture system. These results indicate that HuD-sv4 might play a role other than promoting neuronal marker expression. To determine the role of HuD-sv4, its effect on proliferation was investigated. Because epithelial cells were not suitable for evaluating proliferation, N1E-115 cells were used. In N1E-115 cells, HuD-sv4 overexpression strongly suppressed cell proliferation compared with HuD-sv1, which also showed a strong tendency to suppress proliferation ($P = 0.06$). By contrast, HuD-sv4 induced neurite outgrowth. It was unclear why HuD-sv4 showed induction in these cells but not in neural epithelial cells. However, the induction by HuD-sv4 was clearly weaker than that by HuD-sv1 in both N1E-115 and neural epithelial cells. Overall, these results suggest that HuD SVs have similar functions but alternative effects on neuronal differentiation and growth arrest.

Differences in Intercellular Localization of HuD SVs

This study demonstrates that HuD-sv2 and -sv4 exist in the cytoplasm and nuclei, whereas HuD-sv1 exists in the cytoplasm. The alignment analysis of HuD SVs with HuA, HuB, and HuC revealed that linker regions of HuD-sv2 and HuD-sv4 are extremely similar to HuB and HuA, respectively (Fig. 1A). HuB was previously found to localize primarily in the cytoplasm, whereas HuA was localized in nuclei (Colombrita et al., 2013), so we speculated that HuD-sv2 would localize primarily in the cytoplasm and that HuD-sv4 would localize in the nuclei. However, HuD-sv2 and -sv4 were localized in both the cytoplasm and the nuclei. Considering these results and the fact that HuC localizes in the cytoplasm (Colombrita et al., 2013), we then hypothesized that the intracellular localization of HuD proteins might be regulated by 263R (Ser in HuB and HuC instead of Arg) and by 277R. 263R and 277R are maintained in HuD-sv1, HuB, and HuC (Fig. 1A) but are only partially present or are not present in HuD-sv2 or -sv4. Most likely, the loss of these amino acids diminishes NES activity and suppresses HuD export from nuclei, resulting in cytoplasmic and nucleic localization of HuD-sv2 and -sv4. This hypothesis requires further confirmation.

Relationship Between the Intracellular Localization and Translational Activity of HuD SVs

Translation occurs in the cytoplasm; therefore, the cytoplasmic localization of HuD SVs should lead to subsequent translational upregulation. In fact, HuD-sv1 showed strong translational activation of p21 mRNA. However, HuD-sv4 did not show this activity, although HuD-sv4

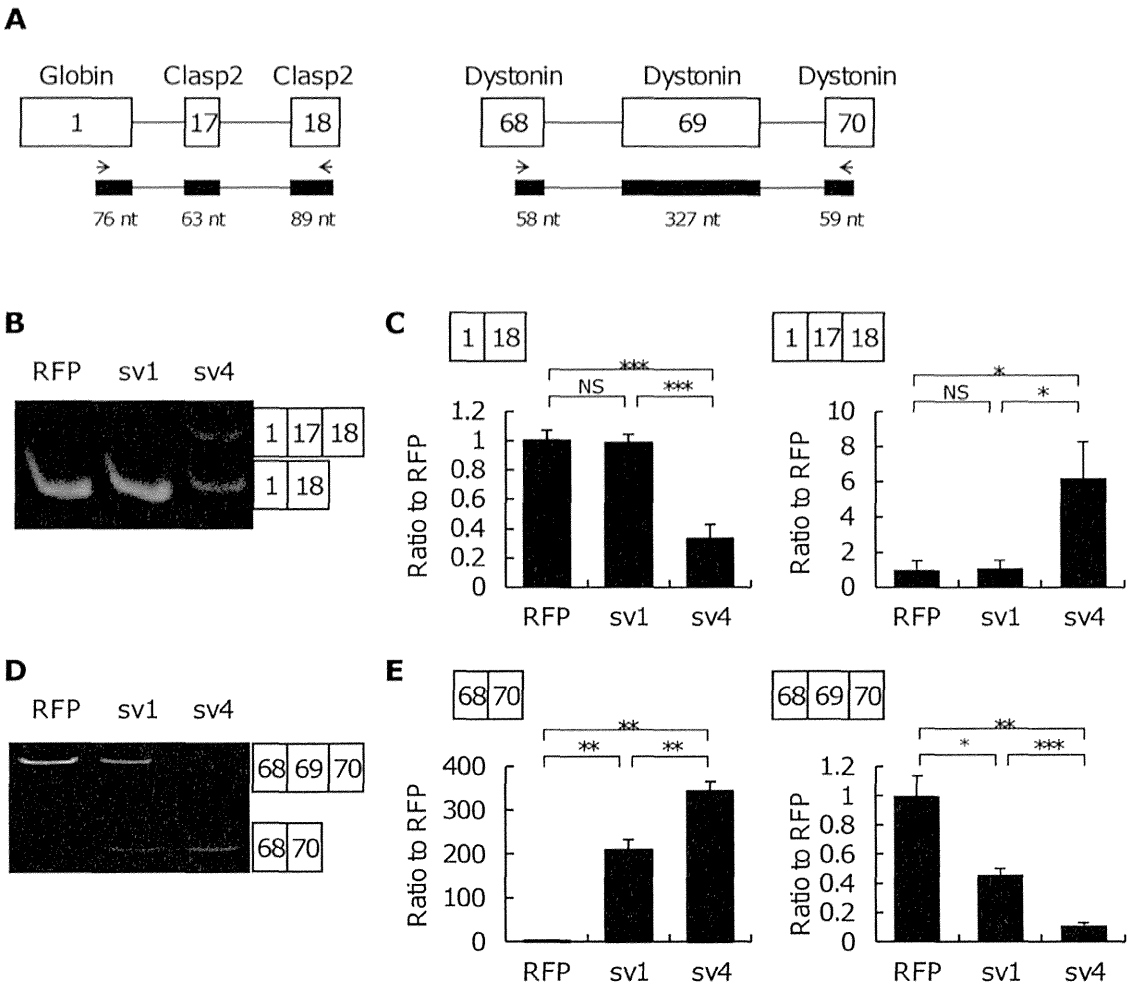

Fig. 6. mRNA splicing activities of HuD-sv1 and -sv4. **A:** Construct of splicing reporters of Clasp2 and Dystonin. **B–E:** Reporter genes of Clasp2 (B) or Dystonin (D) were cotransfected into 293T cells with the HuD SVs or with the RFP control. Spliced mRNA was extracted and subjected to RT-PCR with specific primer pairs (arrows in A). The intensity of each band was quantified in ImageJ (C,E). The values represent mean ± SD. $*P < 0.05$, $**P < 0.01$, $***P < 0.001$, Student's t-test or Welch's test. NS: not significantly separated.

also existed to some extent in the cytoplasm. Thus, the differences in the translational modulating activity of HuD SVs could not be accounted for by their cytoplasmic localization. One possibility for these differences is the uniqueness of their target mRNAs. In the case of p21, HuD-sv4 showed weak activity; however, whether HuD-sv4 will show translational activity on another mRNA target is an important question that remains to be addressed. Another possibility is that there are differences among the HuD SVs in their affinities for their binding partners. Recently, HuD-sv1 was shown to stimulate cap-dependent translation in a poly(A)- and eIF4A-dependent manner, and amino acid 278F of HuD-sv1 is important for the association of HuD-sv1 and eIF4A (Fukao et al., 2009). 278F is the amino acid that is upstream of NES, and HuD-sv4 lacks the amino acids between 251L and 277R. Therefore, we speculate that the lack of the amino acids might affect the conformation or another characteristic of HuD-sv4 and alter the association of HuD-sv4 with eIF4A, which would account for the lower translational activity of HuD-sv4 despite its partial existence in the cytoplasm.

Relationship Between the Intercellular Localization and the Alternative Splicing Activity of HuD SVs

Alternative splicing of several pre-mRNAs by Hu proteins has been demonstrated in fly and mammalian nervous systems (Ince-Dunn et al., 2012; Colombrita et al., 2013). Splicing by the neuronal Hu protein was first shown by the neuron-specific production of calcitonin/calcitonin gene-related peptide (CGRP; Zhu et al., 2006). HuC competitively bound to an intronic U-rich

TABLE I. Summary of Each HuD Splice Variant*

		HuD-sv1	HuD-sv2	HuD-sv4
Differentiation†	Epithelial cells	100	Not tested	20
	N1E-115 cells	1,487	1,232	7,93
Proliferation‡		−51	−87	−98
Localization§	Cytoplasm	++	+	+
	Nucleus	−	+	+
Translation†		78	Not tested	3
Splicing†	Clasp2	−2	Not tested	−67
	Dystonin	20,689	Not tested	34,169

*Change (%) from each control.
†[Ratio (%) to each control] − 100%.
‡([Growth ratio (day 3/day 1)]$_{\text{each variant}}$ − 1)/([growth ratio (day 3/day 1)]$_{\text{mock}}$ − 1) × 100.
§++, Dominant; +, intermediate; −, low.
Clasp2: Clasp2 excluding exon 17, Dystonin: Dystonin excluding exon 69.

sequence and released TIA-1 and TIAR, which are other splicing factors, and promoted the skipping of exon 4 of calcitonin/CGRP pre-mRNA (Zhu et al., 2006). Recently, exon 6 of HuD itself was found to be alternatively spliced by HuB, HuC, and HuD SVs, and HuD-sv4 generated more mRNA, including exon 6, than HuD-sv1 and -sv2 (Wang et al., 2010). Additionally, in this study both HuD-sv1 and -sv4 clearly showed alternative splicing activity, and HuD-sv4 showed stronger activity on Clasp2 and Dystonin than did HuD-sv1. This study reveals that HuD-sv4 has a unique target pre-mRNA, Clasp2, which is not processed by HuD-sv1. What causes the difference in alternative splicing activity in HuD SVs? One possibility is the modified localization of HuD SVs. All HuD SVs have both NLS and NES (Fig. 1A) and can shuttle between the cytoplasm and nuclei, similarly to HuD-sv1. HuD-sv2 and -sv4 localized in the cytoplasm and nuclei, indicating the tendency for nucleic localization compared with HuD-sv1. The nuclear localization would provide a greater opportunity for alternative splicing than cytoplasmic localization, because splicing occurs in the nucleus. Concomitant with this finding, HuD-sv4 showed stronger splicing activity than HuD-sv1. Other possibilities, such as different affinities for binding partners, remain to be evaluated.

Functions of HuD SVs

As summarized in Table I, HuD-sv1 and -sv4 showed variable activities regarding neuronal differentiation, cell proliferation, intracellular localization, translation, and alternative splicing. Among these activities, translation and alternative splicing are key points accounting for the differences in the promotion of neuronal differentiation and cell growth by HuD SVs. Neuronal Hu stabilizes numerous ARE-containing mRNAs, which code for essential proteins in neuronal differentiation, and upregulates their translation (Colombrita et al., 2013), and HuD alternatively splices numerous pre-mRNAs that play roles in proliferation and differentiation (Ince-Dunn et al., 2012). Therefore, the phenotypes of cells that are differentiating, proliferating, or undergoing neither process might be according to the results of the translational and splicing variations of target genes and cannot be described separately. The genes used in this study for evaluating translational and alternative splicing activities are also known to play roles, or have been suggested to play roles, in neuronal differentiation and cell proliferation (Tanaka et al., 2002; Yano et al., 2005; Al-Bassam and Chang, 2011; Ferrier et al., 2013). Most likely, these genes are involved in the control of neuronal differentiation and cell proliferation by HuD SVs. This study showed that HuD-sv4 was transiently expressed in neural development. The expression level was likely not so high; however, HuD-sv4 targeted a gene that HuD-sv1 did not, indicating that HuD-sv4 has its own role. These results indicate that HuD generates diversity in its action by the functions of its SVs. The amounts that individual target genes contribute to these phenotypes remain to be elucidated. Here, translational and alternative splicing activities of HuD-sv2 were not addressed. Given that HuD-sv2 has similar intracellular localization to HuD-sv4 (Fig. 4) but has intermediate activities in neuronal differentiation and growth arrest compared with HuD-sv1 and -sv4 (Fig. 3), HuD-sv2 could have its own targets or different activities on translation and alternative splicing. These results provide further insight into the detailed function of HuD in neural development.

Above all, HuD-sv1 strongly promoted neurite outgrowth or neuronal differentiation, whereas HuD-sv4 had a weaker effect. Additionally, HuD-sv1 moderately suppressed the cell cycle, whereas HuD-sv4 had a stronger inhibitory effect on the cell cycle. The altered translational activity could be caused by intracellular localization and by binding partners, such as eIF4A. The mechanism of this alternative splicing activity might depend on nuclear localization but remains to be elucidated. In conclusion, HuD-sv4 has distinct properties from HuD-sv1, which is the general form of HuD. HuD-sv1 and -sv4 specifically differ in the timing of expression, promotion of neuronal differentiation, induction of cell cycle arrest, intracellular localization, translation, and alternative splicing. HuD SVs might control target genes through a variety of actions related to altered translation and alternative splicing, which might contribute to the complicated regulation of the neuronal differentiation process.

ACKNOWLEDGMENTS

The authors thank Dr. S. Mitani for the kind gift of anti-green fluorescent protein mouse monoclonal IgG, Dr. H. Miyoshi for the kind gift of lentivirus vectors, and Dr. Y. Okada for technical advice and valuable discussions. The authors also thank Drs. M. Miyamoto, H. Nagaya, M. Sakai, A. Nakanishi, S. Morita, H. Matsui, and N. Koyama for their support.

REFERENCES

Akamatsu W, Okano HJ, Osumi N, Inoue T, Nakamura S, Sakakibara S, Miura M, Matsuo N, Darnell RB, Okano H. 1999. Mammalian ELAV-like neuronal RNA-binding proteins HuB and HuC promote neuronal development in both the central and the peripheral nervous systems. Proc Natl Acad Sci U S A 96:9885–9890.

Al-Bassam J, Chang F. 2011. Regulation of microtubule dynamics by TOG-domain proteins XMAP215/Dis1 and CLASP. Trends Cell Biol 21:604–614.

Antic D, Lu N, Keene JD. 1999. ELAV tumor antigen, Hel-N1, increases translation of neurofilament M mRNA and induces formation of neurites in human teratocarcinoma cells. Genes Dev 13:449–461.

Aranda-Abreu GE, Behar L, Chung S, Furneaux H, Ginzburg I. 1999. Embryonic lethal abnormal vision-like RNA-binding proteins regulate neurite outgrowth and tau expression in PC12 cells. J Neurosci 19: 6907–6917.

Blencowe BJ. 2006. Alternative splicing: new insights from global analyses. Cell 126:37–47.

Chung S, Eckrich M, Perrone-Bizzozero N, Kohn DT, Furneaux H. 1997. The Elav-like proteins bind to a conserved regulatory element in the 3′-untranslated region of GAP-43 mRNA. J Biol Chem 272:6593–6598.

Colombrita C, Silani V, Ratti A. 2013. ELAV proteins along evolution: back to the nucleus? Mol Cell Neurosci 56:447–455.

Dalmau J, Furneaux HM, Cordon-Cardo C, Posner JB. 1992. The expression of the Hu (paraneoplastic encephalomyelitis/sensory neuronopathy) antigen in human normal and tumor tissues. Am J Pathol 141:881–886.

Darnell RB. 2002. RNA logic in time and space. Cell 110:545–550.

Fan XC, Steitz JA. 1998. Overexpression of HuR, a nuclear-cytoplasmic shuttling protein, increases the in vivo stability of ARE-containing mRNAs. EMBO J 17:3448–3460.

Ferrier A, Boyer JG, Kothary R. 2013. Cellular and molecular biology of neuronal dystonin. Int Rev Cell Mol Biol 300:85–120.

Fukao A, Sasano Y, Imataka H, Inoue K, Sakamoto H, Sonenberg N, Thoma C, Fujiwara T. 2009. The ELAV protein HuD stimulates cap-dependent translation in a poly(A)- and eIF4A-dependent manner. Mol Cell 36:1007–1017.

Good PJ. 1995. A conserved family of elav-like genes in vertebrates. Proc Natl Acad Sci U S A 92:4557–4561.

Good PJ. 1997. The role of elav-like genes, a conserved family encoding RNA-binding proteins, in growth and development. Semin Cell Dev Biol 8:577–584.

Gorospe M, Wang X, Holbrook NJ. 1998. p53-Dependent elevation of p21Waf1 expression by UV light is mediated through mRNA stabilization and involves a vanadate-sensitive regulatory system. Mol Cell Biol 18:1400–1407.

Homyk T, Jr., Isono K, Pak WL. 1985. Developmental and physiological analysis of a conditional mutation affecting photoreceptor and optic lobe development in *Drosophila melanogaster*. J Neurogenet 2:309–324.

Imai T, Tokunaga A, Yoshida T, Hashimoto M, Mikoshiba K, Weinmaster G, Nakafuku M, Okano H. 2001. The neural RNA-binding protein Musashi1 translationally regulates mammalian numb gene expression by interacting with its mRNA. Mol Cell Biol 21:3888–3900.

Ince-Dunn G, Okano HJ, Jensen KB, Park WY, Zhong R, Ule J, Mele A, Fak JJ, Yang C, Zhang C, Yoo J, Herre M, Okano H, Noebels JL, Darnell RB. 2012. Neuronal Elav-like (Hu) proteins regulate RNA splicing and abundance to control glutamate levels and neuronal excitability. Neuron 75:1067–1080.

Joseph B, Orlian M, Furneaux H. 1998. p21(waf1) mRNA contains a conserved element in its 3′-untranslated region that is bound by the Elav-like mRNA-stabilizing proteins. J Biol Chem 273:20511–20516.

Kasashima K, Terashima K, Yamamoto K, Sakashita E, Sakamoto H. 1999. Cytoplasmic localization is required for the mammalian ELAV-like protein HuD to induce neuronal differentiation. Genes Cells 4:667–683.

Kullmann M, Gopfert U, Siewe B, Hengst L. 2002. ELAV/Hu proteins inhibit p27 translation via an IRES element in the p27 5′UTR. Genes Dev 16:3087–3099.

Levine TD, Gao F, King PH, Andrews LG, Keene JD. 1993. Hel-N1: an autoimmune RNA-binding protein with specificity for 3′ uridylate-rich untranslated regions of growth factor mRNAs. Mol Cell Biol 13: 3494–3504.

Ma WJ, Cheng S, Campbell C, Wright A, Furneaux H. 1996. Cloning and characterization of HuR, a ubiquitously expressed Elav-like protein. J Biol Chem 271:8144–8151.

Miyoshi H, Blomer U, Takahashi M, Gage FH, Verma IM. 1998. Development of a self-inactivating lentivirus vector. J Virol 72:8150–8157.

Nagai T, Ibata K, Park ES, Kubota M, Mikoshiba K, Miyawaki A. 2002. A variant of yellow fluorescent protein with fast and efficient maturation for cell-biological applications. Nat Biotechnol 20:87–90.

Niwa H, Yamamura K, Miyazaki J. 1991. Efficient selection for high-expression transfectants with a novel eukaryotic vector. Gene 108:193–199.

Okabe M, Imai T, Kurusu M, Hiromi Y, Okano H. 2001. Translational repression determines a neuronal potential in *Drosophila* asymmetric cell division. Nature 411:94–98.

Okano HJ, Darnell RB. 1997. A hierarchy of Hu RNA binding proteins in developing and adult neurons. J Neurosci 17:3024–3037.

Okano H, Imai T, Okabe M. 2002. Musashi: a translational regulator of cell fate. J Cell Sci 115:1355–1359.

Ostareck DH, Ostareck-Lederer A, Wilm M, Thiele BJ, Mann M, Hentze MW. 1997. mRNA silencing in erythroid differentiation: hnRNP K and hnRNP E1 regulate 15-lipoxygenase translation from the 3′ end. Cell 89:597–606.

Robinow S, Campos AR, Yao KM, White K. 1988. The elav gene product of *Drosophila*, required in neurons, has three RNP consensus motifs. Science 242:1570–1572.

Sakai K, Gofuku M, Kitagawa Y, Ogasawara T, Hirose G, Yamazaki M, Koh CS, Yanagisawa N, Steinman L. 1994. A hippocampal protein associated with paraneoplastic neurologic syndrome and small cell lung carcinoma. Biochem Biophys Res Commun 199:1200–1208.

Szabo A, Dalmau J, Manley G, Rosenfeld M, Wong E, Henson J, Posner JB, Furneaux HM. 1991. HuD, a paraneoplastic encephalomyelitis antigen, contains RNA-binding domains and is homologous to Elav and Sex-lethal. Cell 67:325–333.

Tanaka H, Yamashita T, Asada M, Mizutani S, Yoshikawa H, Tohyama M. 2002. Cytoplasmic p21(Cip1/WAF1) regulates neurite remodeling by inhibiting rho-kinase activity. J Cell Biol 158:321–329.

Tenenbaum SA, Carson CC, Lager PJ, Keene JD. 2000. Identifying mRNA subsets in messenger ribonucleoprotein complexes by using cDNA arrays. Proc Natl Acad Sci U S A 97:14085–14090.

Wang ET, Sandberg R, Luo S, Khrebtukova I, Zhang L, Mayr C, Kingsmore SF, Schroth GP, Burge CB. 2008. Alternative isoform regulation in human tissue transcriptomes. Nature 456:470–476.

Wang H, Molfenter J, Zhu H, Lou H. 2010. Promotion of exon 6 inclusion in HuD pre-mRNA by Hu protein family members. Nucleic Acids Res 38:3760–3770.

Wang W, Furneaux H, Cheng H, Caldwell MC, Hutter D, Liu Y, Holbrook N, Gorospe M. 2000. HuR regulates p21 mRNA stabilization by UV light. Mol Cell Biol 20:760–769.

Yano M, Okano HJ, Okano H. 2005. Involvement of Hu and heterogeneous nuclear ribonucleoprotein K in neuronal differentiation through p21 mRNA posttranscriptional regulation. J Biol Chem 280:12690–12699.

Yano M, Hayakawa-Yano Y, Mele A, Darnell RB. 2010. Nova2 regulates neuronal migration through an RNA switch in disabled-1 signaling. Neuron 66:848–858.

Zhu H, Hasman RA, Barron VA, Luo G, Lou H. 2006. A nuclear function of Hu proteins as neuron-specific alternative RNA processing regulators. Mol Biol Cell 17:5105–5114.

NEUROPATHOLOGY

Neuropathology 2014; **34**, 135–139 doi:10.1111/neup.12069

Original Article

Immunohistochemical localization of spatacsin in α-synucleinopathies

Satoshi Kuru,[1] Mari Yoshida,[2] Shinsui Tatsumi[2] and Maya Mimuro[2]

[1]Department of Neurology, National Organization Suzuka Hospital, Suzuka and [2]Department of Neuropathology, Institute for Medical Science of Aging, Aichi Medical School, Aichi, Japan

***Spatacsin* (SPG11) is a major mutated gene in autosomal recessive spastic paraplegia with thin corpus callosum (ARHSP-TCC) and is responsible for juvenile Parkinsonism. To elucidate the role of spatacsin in the pathogenesis of α-synucleinopathies, an immunohistochemical investigation was performed on the brain of patients with Parkinson's disease (PD), dementia with Lewy bodies (DLB) and multiple system atrophy (MSA) using anti-spatacsin antibody. In PD, Lewy bodies (LBs) in the brain stem were positive for spatacsin. These LBs showed intense staining in their peripheral portions and occasionally in the central cores. Lewy neurites were also spatacsin-positive. In DLB, cortical LBs were immunolabeled by spatacsin. In MSA, glial cytoplasmic inclusions (GCI) and a small fraction of neuronal cytoplasmic inclusions (NCI) were positive for spatacsin. The widespread accumulation of spatacsin observed in pathologic α-synuclein-containing inclusions suggests that spatacsin may be involved in the pathogenesis of α-synucleinopathies.**

Key words: α-synucleinopathies, glial cytoplasmic inclusions, immunohistochemistry, Lewy bodies, spatacsin.

INTRODUCTION

Spatacsin (*SPG11*) is a major mutated gene in autosomal recessive hereditary spastic paraplegia with thin corpus callosum (ARHSP-TCC).[1–4] The *SPG11* gene contains 40 exons on chromosome 15q21.1, and encodes a 2443 amino acid protein, spatacsin, with an unknown biological function.[4] Spatacsin is highly conserved among species and ubiquitously expressed in the nervous system, particularly in the cerebellum, cerebral cortex and hippocampus.[5] Because knockdown of SPG11 during Zebrafish development is characterized by CNS development defects, it is considered to have an important biological function.[3] Anheim reported two patients of Turkish origin affected with SPG11 in association with early-onset parkinsonism. In those cases, dopaminergic denervation was confirmed by ^{123}I-ioflupane SPECT.[6] Additional evidence suggested that the mutation of *SPG11* could cause early-onset levodopa-responsive parkinsonism with pyramidal signs.[7] We postulated that spatacsin might be involved in the pathogenesis of Parkinson's disease (PD). In the present study, we performed immunohistochemical studies on the brains of patients with PD, dementia with Lewy bodies (DLB) and multiple system atrophy (MSA) to elucidate the role of spatacsin in the pathogenesis of α-synucleinopathies.

MATERIALS AND METHODS

We examined the autopsied brain tissues of five PD patients (age: 66–84 years), five DLB patients (56–90 years), four MSA patients (61–81 years), and four control subjects (61–71 years). All the diagnoses had been confirmed both clinically and neuropathologically. The antibodies used were polyclonal antibodies against spatacsin (Novus Biologicals, NBP1-71668, Littleton, CO, USA, 1:200) and phosphorylated α-synuclein (WAKO, Osaka, Japan, 1:6000). In each case, 6-μm-thick sections of the temporal lobe, midbrain, and upper pons were excised. For immunohistochemistry, formalin-fixed paraffin-embedded sections were deparaffinized with xylene and hydrated in ethanol. Antigen unmasking was performed by placing slides in 1% citrate buffer at 95°C for 40 min. Endogenous peroxidases were quenched by incubation with 3% hydrogen peroxide for 5 min. Sections were then treated at 4°C for 1 h with a primary antibody. After treatment with the primary antibody, sections were incubated with biotinylated anti-rabbit IgG from goats (Dako

Correspondence: Satoshi Kuru, MD, Department of Neurology, National Organization Suzuka Hospital, 3-2-1, Kasado, Suzuka, Mie 513-8501, Japan. Email: kuru@suzuka.hosp.go.jp

Received 3 June 2013; revised and accepted 19 August 2013; published online 22 September 2013.

Corporation, Carpinteria, CA, USA; diluted 1:100) or with biotinylated anti-mouse IgG also from goats (Dako Corporation; diluted 1:100) as the second antibody. Sections were visualized with the avidin-biotinylated peroxidase complex (ABC Elite kit, Vector Laboratories, Burlingame, CA, USA) and 3,3′-diaminobenzidine (DAB, Wako Pure Chemical Industries, Osaka, Japan). Their nuclei were stained using the hematoxylin method. For the absorption experiments, 50 μg/mL of anti-spatacsin antibody was incubated with 13.5 μg/mL of blocking peptide (NBP1-76990PEP, Novus Biologicals) for 24 h at 4°C prior to application to tissue sections.

Double immunofluorescence was performed using a mouse monoclonal antibody against α-synuclein (1:600), and a rabbit polyclonal antibody against spatacsin (1:60). The second antibodies used were Alexa Fluor 488 goat anti-mouse IgG (Molecular Probes, Eugene, OR, USA; diluted 1:250) and Alexa Fluor 568 goat anti-rabbit IgG (Molecular Probes; diluted 1:250). The signal was observed under a Carl Zeiss LSM-710 laser scanning confocal microscope (Carl Zeiss, Oberkochen, Germany).

Spatacsin positivity in LBs and glial cytoplasmic inclusions (GCIs)

LBs and GCIs are confirmed by anti-α-synuclein. Serial sections were then immunolabeled for spatacsin and immunopositivity for spatacsin was calculated.

RESULTS

Immunorecognition of the antibody was specific since prior absorption of the antibody reduced the immunoreactivity (Fig. 1A–C). In the control sample, anti-spatacsin antibodies immunostained the cytoplasm of neurons of the oculomotor nucleus (Fig. 1D). LBs observed in the substantia nigra were positive for spatacsin in PD. Spatacsin immunolabeling was identified in the peripheral zone and less frequently in the central core of LBs (Fig. 1E,F). Lewy neurites also showed homogeneous immunoreactivities for spatacsin (Fig. 1G). Pale bodies were heterogeneously immunolabeled (Fig. 1H). Spatacsin-positive glial inclusions were observed (Fig. 1G). Semiquantitative data on percentages of spatacsin-immunopositive LBs are summarized in Table 1. In DLB, cortical LBs were immunolabeled by spatacsin (Fig. 1I). In MSA, numerous GCIs and a small fraction of neuronal cytoplasmic inclusions (NCI) were positive for spatacsin (Fig. 1J,K).

To confirm the presence of spatacsin in LBs and GCIs, we performed double immunofluorescence staining with anti-spatacsin and α-synuclein antibodies. We found a colocalization of spatacsin and α-synuclein immunolabeling in the inner part of the peripheral halo region of brainstem-type LBs. The core region of some LBs was spatacsin-positive but α-synuclein-negative, while the outer halves of the halo region of LBs were

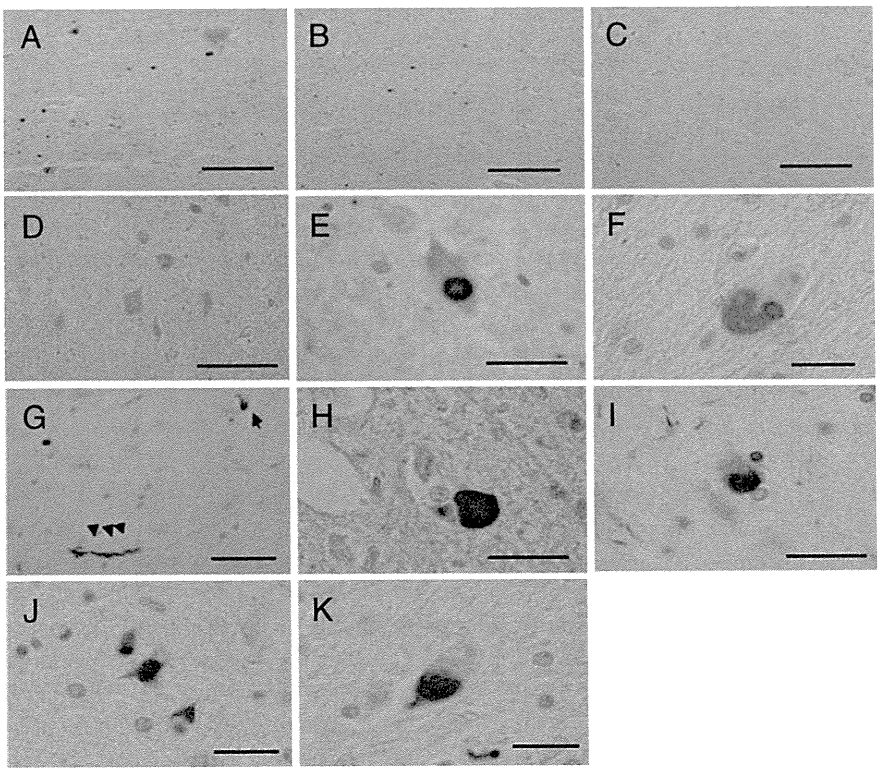

Fig. 1 Spatacsin immunoreactivity in the brain of normal controls (D), patients with Parkinson's disease (A–C,E,F), dementia with Lewy bodies (DLB) (G), and multiple system atrophy (H,I). Locus ceruleus sections were immunostained with α-synuclein (A) and spatacsin (B). As a negative control, spatacsin antibody was absorbed with blocking peptide and supernatant fractions were then used in parallel immunohistochemical analysis (C). Neuronal cytoplasm of the oculomotor nuclei is weakly immunostained (D). Substantia nigra sections were immunostained with spatacsin antibody (E,F). Spatacsin immunolabeling was identified in the peripheral zone (E), occasionally in the central core of LBs (F). Spatacsin-positive staining in Lewy neurites (arrowhead) and glial inclusions (arrow) (G). Pale bodies were heterogeneously immunolabeled (Fig. 1H). Spatacsin-positive cortical LBs in amygdala of diffuse LB disease brains (I). Spatacsin-positive glial cytoplasmic inclusions in the pontine base (J). Spatacsin-positive neuronal cytoplasmic inclusions in the pontine base (K). A–C: scale bar = 200 μm; D,G: scale bar = 100 μm, E,F,H–K: scale bar = 20 μm.

Table 1 Summary of cases

Patient	Age/sex	Diagnosis	Spatacsin+/total LBs (%)			Spatacsin+/total GCIs (%)
			Substantia nigra	Locus coeruleus	Temporal cortex	Pons
1	84/F	PD	25/45 (55.5)	33/60 (55.0)		
2	73/M	PD	48/56 (85.7)	20/52 (38.5)		
3	73/M	PD	21/40 (52.5)	36/52 (69.2)		
4	66/M	PD	46/46 (100)	20/52 (38.5)		
5	83/M	PD	45/54 (83.3)	15/57 (26.3)		
6	56/F	DLB	20/45 (44.4)	39/54 (72.2)	7/50 (14.0)	
7	90/M	DLB	28/56 (50.0)	28/54 (51.9)	19/106 (16.9)	
8	92/F	DLB	12/52 (23.1)	10/54 (18.5)	6/73 (8.2)	
9	72/F	DLB	32/52 (61.5)	14/52 (26.9)	38/92 (41.3)	
10	72/M	DLB	10/52 (19.2)	42/51 (82.4)	12/62 (19.3)	
11	81/M	MSA				88/104 (84.6)
12	61/M	MSA				130/138 (94.2)
13	80/F	MSA				75/138 (54.3)
14	70/M	MSA				40/93 (43.0)

GCI, glial cytoplasmic inclusions; PD, Parkinson's disease; DLB, dementia with Lewy bodies; MSA, multiple system atrophy.

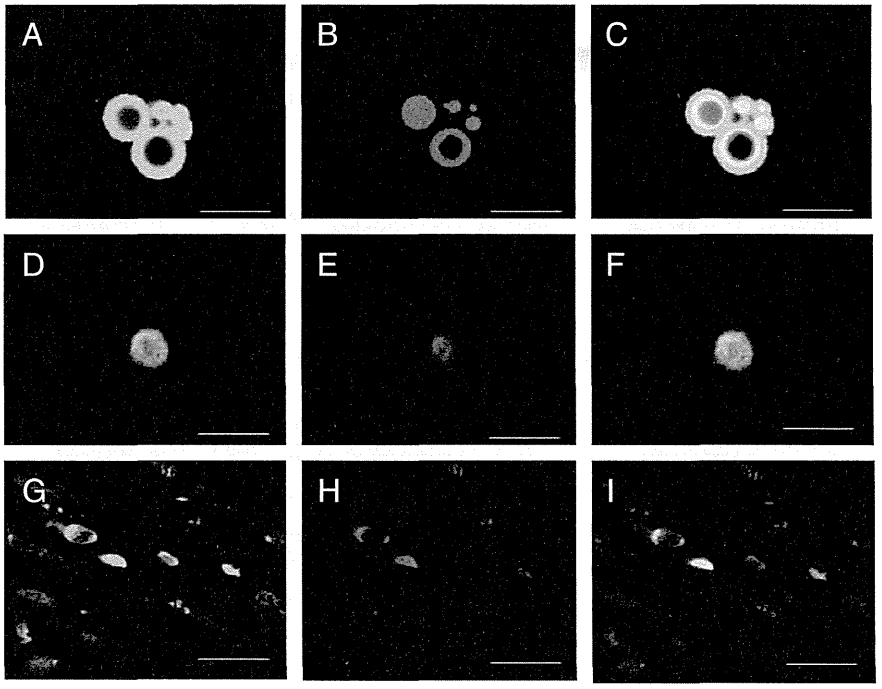

Fig. 2 Double immunofluorescence staining for α-synuclein (A,D,G) and spatacsin (B,E,H) in the substantia nigra from a patient with Parkinson disease (PD) (A–C), in the amygdala from a patient with dementia with Lewy bodies (DLB) (D–F), basis pontis from a patient with multiple system atrophy (MSA) (G–I). The merged images showed that α-synuclein and spatacsin were colocalized in brainstem-type Lewy bodies (C), cortical Lewy body (F) and glial cytoplasmic inclusions (I). A–C: scale bar = 10 μm; D–I: scale bar = 20 μm.

spatacsin-negative but α-synuclein-positive (Fig. 2A–C). Colocalization of spatacsin and α-synuclein immunolabeling was observed in the central core portion of LBs in the amygdala (Fig. 2D–F).

DISCUSSION

In this study, we identified spatacsin as a component of LBs and GCIs. To the best of our knowledge, this is the first report demonstrating the detailed distribution of spatacsin immunoreactivity in α-synucleinopathies. In the present study, the central cores of some LBs contain spatacsin. The cores of LBs are composed mainly of densely packed vesicular structures. Synphilin is a major component of LBs and located in the central core.[8] Parkin, identified as a ubiquitin ligase (E3), is also a component of LBs.[9] Both proteins were reported to show overlapping expression pattern and form aggresomes in response to proteasomal inhibition.[10] However, the interaction of spatacsin with synphilin and parkin remains unknown. We also observed spatacsin immunoreactivity in pale bodies, which are considered to be precursors of LBs, suggesting that spatacsin may be involved in the formation of LBs in the early stages.

The mechanism of LB formation remains to be elucidated. α-synuclein is a major constituent of LBs.[11–13] More than 70 molecules have been detected in LBs. Among these components, several proteins, such as α-synuclein, DJ-1, leucine-rich repeat kinase 2, parkin and PINK-1, are PD-related gene products.[14] Recent reports have shown that the mutation of spatacsin caused juvenile-onset Parkinsonism.[6,7] However, why some *SPG11* mutations lead to parkinsonism remains unknown. The already reported parkinsonism-related mutations in *SPG11* were distributed throughout the gene.[6,7] Thus, no clear correlation between genotype and phenotype has yet been established.

Spatacsin has recently been reported to be phosphorylated upon DNA damage by ataxia telangiectasia mutated (ATM) and ATM and Rad3-related (ATR).[15] ATM is a member of the phosphatidylinositol-3 kinase family that plays a role in the cellular response to DNA double-strand breaks. Camins has demonstrated that 1-methyl-4-phenylpyridinium (MPP^+)-induced DNA damage is followed by ATM activation in an experimental model of PD, and that ATM is also activated in human PD.[16] Indeed, retinoblastoma protein, one of the downstream substrates phosphorylated by ATM, has been identified in the LBs.[17] Together with our findings of spatacsin localization in LB, spatacsin may also be involved in the pathogenesis of PD as a member of proteins that are phosphorylated when DNA is damaged through interaction with ATM.

GCI represents the pathological hallmark of MSA. Although α-synuclein is a major component of GCI, the precise molecular composition of GCI remains to be clarified. The widespread accumulation of spatacsin observed in pathologic α-synuclein-containing inclusions suggests that spatacsin may be involved in the pathogenesis of α-synucleinopathies. Further research on the interaction between spatacsin and α-synuclein is essential for achieving a better understanding of α-synucleinopathies.

ACKNOWLEDGMENT

The authors have no conflict of interest to declare.

REFERENCES

1. Hehr U, Bauer P, Winner B *et al.* Long-term course and mutational spectrum of spatacsin-linked spastic paraplegia. *Ann Neurol* 2007; **62**: 656–665.
2. Paisan-Ruiz C, Dogu O, Yilmaz A, Houlden H, Singleton A. SPG11 mutations are common in familial cases of complicated hereditary spastic paraplegia. *Neurology* 2008; **70**: 1384–1389.
3. Southgate L, Dafou D, Hoyle J *et al.* Novel SPG11 mutations in Asian kindreds and disruption of spatacsin function in the zebrafish. *Neurogenetics* 2010; **211**: 379–389.
4. Stevanin G, Azzedine H, Denora P *et al.* Mutations in SPG11 are frequent in autosomal recessive spastic paraplegia with thin corpus callosum, cognitive decline and lower motor neuron degeneration. *Brain* 2008; **131**: 772–784.
5. Murmu RP, Martin E, Rastetter A *et al.* Cellular distribution and subcellular localization of spatacsin and spastizin, two proteins involved in hereditary spastic paraplegia. *Mol Cell Neurosci* 2011; **47**: 191–202.
6. Anheim M, Lagier-Tourenne C, Stevanin G *et al.* SPG11 spastic paraplegia. A new cause of juvenile parkinsonism. *J Neurol* 2009; **256**: 104–108.
7. Guidubaldi A, Piano C, Santorelli FM *et al.* Novel mutations in SPG11 cause hereditary spastic paraplegia associated with early-onset levodopa-responsive Parkinsonism. *Mov Disord* 2011; **26**: 553–556.
8. Wakabayashi K, Engelender S, Yoshimoto M, Tsuji S, Ross CA, Takahashi H. Synphilin-1 is present in Lewy bodies in Parkinson's disease. *Ann Neurol* 2000; **47**: 521–523.
9. Schlossmacher MG, Frosch MP, Gai WP *et al.* Parkin localizes to the Lewy bodies of Parkinson disease and dementia with Lewy bodies. *Am J Pathol* 2002; **160**: 1655–1667.
10. Bandopadhyay R, Kingsbury AE, Muqit MM *et al.* Synphilin-1 and parkin show overlapping expression patterns in human brain and form aggresomes in response to proteasomal inhibition. *Neurobiol Dis* 2005; **20**: 401–411.
11. Spillantini MG, Schmidt ML, Lee VM, Trojanowski JQ, Jakes R, Goedert M. α-synuclein in Lewy bodies. *Nature* 1997; **388**: 839–840.
12. Baba M, Nakajo S, Tu PH *et al.* Aggregation of α-synuclein in Lewy bodies of sporadic Parkinson's disease and dementia with Lewy bodies. *Am J Pathol* 1998; **152**: 879–884.
13. Fujiwara H, Hasegawa M, Dohmae N *et al.* α-Synuclein is phosphorylated in synucleinopathy lesions. *Nat Cell Biol* 2002; **4**: 160–164.
14. Wakabayashi K, Tanji K, Mori F, Takahashi H. The Lewy body in Parkinson's disease: molecules implicated in the formation and degradation of α-synuclein aggregates. *Neuropathology* 2007; **27**: 494–506.
15. Matsuoka S, Ballif BA, Smogorzewska A *et al.* ATM and ATR substrate analysis reveals extensive protein networks responsive to DNA damage. *Science* 2007; **316**: 1160–1166.

16. Camins A, Pizarro JG, Alvira D, Gutierrez-Cuesta J *et al.* Activation of ataxia telangiectasia muted under experimental models and human Parkinson's disease. *Cell Mol Life Sci* 2010; **67**: 3865–3882.

17. Jordan-Sciutto KL, Dorsey R, Chalovich EM, Hammond RR, Achim CL. Expression patterns of retinoblastoma protein in Parkinson disease. *J Neuropathol Exp Neurol* 2003; **62**: 68–74.

BMJ Open

Differential motor neuron involvement in progressive muscular atrophy: a comparative study with amyotrophic lateral sclerosis

Yuichi Riku,[1] Naoki Atsuta,[1] Mari Yoshida,[2] Shinsui Tatsumi,[2] Yasushi Iwasaki,[2] Maya Mimuro,[2] Hirohisa Watanabe,[1] Mizuki Ito,[1] Jo Senda,[1] Ryoichi Nakamura,[1] Haruki Koike,[1] Gen Sobue[1]

To cite: Riku Y, Atsuta N, Yoshida M, *et al*. Differential motor neuron involvement in progressive muscular atrophy: a comparative study with amyotrophic lateral sclerosis. *BMJ Open* 2014;**4**: e005213. doi:10.1136/bmjopen-2014-005213

► Prepublication history and additional material is available. To view please visit the journal (http://dx.doi.org/10.1136/bmjopen-2014-005213).

YR and NA contributed equally.

Received 7 March 2014
Revised 7 April 2014
Accepted 10 April 2014

[1]Department of Neurology, Nagoya University Graduate School of Medicine, Nagoya, Japan
[2]Institute for Medical Science of Aging, Aichi Medical University, Aichi, Japan

Correspondence to
Dr Gen Sobue;
sobueg@med.nagoya-u.ac.jp

ABSTRACT

Objective: Progressive muscular atrophy (PMA) is a clinical diagnosis characterised by progressive lower motor neuron (LMN) symptoms/signs with sporadic adult onset. It is unclear whether PMA is simply a clinical phenotype of amyotrophic lateral sclerosis (ALS) in which upper motor neuron (UMN) signs are undetectable. To elucidate the clinicopathological features of patients with clinically diagnosed PMA, we studied consecutive autopsied cases.

Design: Retrospective, observational.

Setting: Autopsied patients.

Participants: We compared clinicopathological profiles of clinically diagnosed PMA and ALS using 107 consecutive autopsied patients. For clinical analysis, 14 and 103 patients were included in clinical PMA and ALS groups, respectively. For neuropathological evaluation, 13 patients with clinical PMA and 29 patients with clinical ALS were included.

Primary outcome measures: Clinical features, UMN and LMN degeneration, axonal density in the corticospinal tract (CST) and immunohistochemical profiles.

Results: Clinically, no significant difference between the prognosis of clinical PMA and ALS groups was shown. Neuropathologically, 84.6% of patients with clinical PMA displayed UMN and LMN degeneration. In the remaining 15.4% of patients with clinical PMA, neuropathological parameters that we defined as UMN degeneration were all negative or in the normal range. In contrast, all patients with clinical ALS displayed a combination of UMN and LMN system degeneration. CST axon densities were diverse in the clinical PMA group, ranging from low values to the normal range, but consistently lower in the clinical ALS group. Immunohistochemically, 85% of patients with clinical PMA displayed 43-kDa TAR DNA-binding protein (TDP-43) pathology, while 15% displayed fused-in-sarcoma (FUS)-positive basophilic inclusion bodies. All of the patients with clinical ALS displayed TDP-43 pathology.

Conclusions: PMA has three neuropathological background patterns. A combination of UMN and LMN degeneration with TDP-43 pathology, consistent with ALS, is the major pathological profile. The remaining patterns have LMN degeneration with TDP-43 pathology without UMN degeneration, or a combination of UMN and LMN degeneration with FUS-positive basophilic inclusion body disease.

Strengths and limitations of this study

- The characteristics of motor neuron involvement in amyotrophic lateral sclerosis or progressive muscular atrophy were comprihensively described.
- The severity of upper motor neuron involvement was semiquantitatively compared between the clinical groups, and quantitatively surrogated by axonal densities in the corticospinal tract.
- Pathological results clearly indicated the differences of upper motor neuron involvement between the clinical groups.
- To evaluate the entire regions in the motor cortex or the corticospinal tract is not possible.
- We prepared formalin-fixed, paraffin-embedded tissues to quantificate axonal densities in the corticospinal tract. In this protocol, the tissues can be distorted compared with the conventional fixation using glutaraldehyde and Epon. The results can vary more than those from other histological techniques.

INTRODUCTION

Motor neuron disease (MND) constitutes a group of heterogeneous neurodegenerative diseases that are associated with progressive upper motor neuron (UMN) and/or lower motor neuron (LMN) degeneration. A portion of MND cases has genetic causes; however, the majority of MND cases are sporadic and of unknown aetiology. Amyotrophic lateral sclerosis (ALS) constitutes the majority of MND cases. ALS is a clinicopathological disorder that presents with progressive UMN and LMN symptoms/signs. Neuropathologically,

the UMN and LMN systems exhibit neuronal loss and gliosis and Bunina bodies are detected in surviving neurons. Although various immunohistochemical profiles have been identified in patients with ALS, 43-kDa TAR DNA-binding protein (TDP-43) is the major pathological protein in sporadic ALS.[1]

In contrast, MND that presents with LMN symptoms/signs alone occurs in several disorders, including genetically mediated disorders such as, spinal muscular atrophy (SMA), symmetrical axonal neuropathy and spinal and bulbar muscular atrophy (SBMA).[2 3] Additionally, a sporadic and adult-onset LMN disease has been referred to as progressive muscular atrophy (PMA).[3 4] Although the revised El Escorial criteria, the standard diagnostic criteria for ALS, exclude patients who only present with LMN symptoms/signs, several studies have revealed that a subset of patients with clinically diagnosed PMA exhibit the neuropathological hallmarks of ALS. Postmortem histopathological studies have revealed corticospinal tract (CST) degeneration in more than half of the patients with MND clinically limited to LMN symptoms/signs.[5 6] TDP-43-immunoreactive inclusions have been detected in the LMNs and cortical neurons of patients with PMA.[7 8] The disease course of PMA is relentlessly progressive, although somewhat longer than that of ALS.[2 4 9 10]

However, it is unclear whether clinically diagnosed PMA is simply a clinical phenotype of ALS in which UMN symptoms/signs are undetectable. In this study, we investigated the clinicopathological profiles of patients with clinically diagnosed PMA compared with those of patients with clinically diagnosed ALS using a series of consecutive adult-onset sporadic MND autopsy cases.

METHODS

Patients and clinical evaluations

We enrolled 130 consecutive autopsied patients who were clinically diagnosed with and pathologically confirmed as suffering from sporadic, adult-onset MND at the Department of Neuropathology of the Institute for Medical Science of Aging at the Aichi Medical University from January 1998 to December 2010. All of the patients had been clinically evaluated by neurological experts at the Nagoya University Hospital, the Aichi Medical University Hospital or their affiliated hospitals. Permission to perform an autopsy and archive the brain and spinal cord for research purposes was obtained from the patients' relatives by the attending physician after death. We evaluated the clinical profiles of the included patients by retrospectively reviewing case notes written at the time of diagnosis and in an advanced disease stage. Disease onset was defined as the time at which patients became aware of muscle weakness. The inclusion criteria for the patients with MND were as follows: older than 18 years at disease onset; no family history of ALS, PMA, progressive lateral sclerosis, inherited SMA or SBMA or any other neurodegenerative disorder; motor neuron involvement based on neurological examination and neuropathological evidence of neuronal loss and gliosis in the UMN and/or LMN systems that were not due to any cerebrovascular diseases, metabolic disorders, genetic neurological disorders, inflammatory disorders, neoplasms or traumas. We excluded 22 patients due to invalid clinical data and 1 patient with only UMN symptoms/signs throughout his disease course; 107 patients were ultimately included in this study. Based on the clinical data, we separated these 107 patients with MND into two groups, namely the clinical PMA and clinical ALS groups. According to a previous study,[4] clinical PMA was defined by neurological evidence of LMN involvement (decreased or diminished deep tendon reflexes and muscle atrophy) and a lack of UMN symptoms/signs (increased jaw jerk, other exaggerated tendon reflexes, Babinski sign, other pathological reflexes, forced crying and forced laughing) throughout the clinical course. Patients who exhibited motor conduction block(s) based on extensive standardised nerve conduction studies,[11] exhibited objective sensory signs (apart from mild vibration sensory disturbances in elderly patients) or had a history of diseases that may mimic MND (eg, spinal radiculopathy, poliomyelitis and diabetic amyotrophy) were not included in the clinical PMA group.[4] We defined clinical ALS, based on the revised El Escorial criteria, as fulfilling 'possible' or above categories, which require UMN signs/symptoms in at least one region of the body.[12]

Pathological evaluations

For pathological evaluations, we excluded one patient with clinical PMA due to severe anoxic changes in the brain and four patients with clinical ALS due to insufficient tissue material. Ultimately, we enrolled 13 patients with clinical PMA for pathological evaluations. For comparison, we enrolled 29 patients with clinical ALS who were consecutively autopsied during the past 5 years of the study period (after January 2006). Additionally, 13 age-matched controls (mean age at death 68 ±6.91 years) were enrolled. We prepared 8 mm coronal sections of the cerebrum and 5 mm axial sections of the brainstem. The tissues were fixed using 20% neutral-buffered formalin, embedded in paraffin and sectioned at a thickness of 4.5 μm. We evaluated the sections from the precentral gyrus (four segments from the left hemisphere), hippocampus, brainstem and spinal cord. In all cases, the spinal cord was examined at all segment levels. Two investigators (YR and MY) evaluated the degeneration of the motor neuron systems and the immunohistochemical profiles of the included patients. The investigators were completely blinded to each patient's ID and the clinical diagnosis corresponding to each specimen. With respect to the degeneration of motor neuron systems, the severity of motor neuron loss in the primary motor cortex, facial and hypoglossal nuclei and spinal anterior horns, myelin pallor within the CST and aggregation of macrophages within the

primary motor cortex and CST were evaluated. The evaluations were performed on the most severely affected lesions and graded as none (−), mild (+), moderate (++) or severe (+++; figure 1). The immunohistochemical profiles were evaluated using anti-pTDP-43 and antifused-in-sarcoma (FUS) antibodies in the LMN system and cerebrum. For the routine neuropathological examinations, the sections were subjected to H&E or Klüver-Barrera staining. Immunohistochemistry was performed according to a standard polymer-based method using the EnVision Kit (Dako, Glostrup, Denmark). The primary antibodies used in this study were antiubiquitin (polyclonal rabbit, 1:2000; Dako, Glostrup, Denmark), anti-TDP-43 (polyclonal rabbit, 1:2500; ProteinTech, Chicago, Illinois, USA), antiphosphorylated TDP-43 (pTDP-43 ser 409/410, polyclonal rabbit, 1:2500; CosmoBio, Tokyo, Japan), anti-FUS (polyclonal rabbit, 1:500; Sigma Aldrich, St Louis, Missouri, USA), anti-α internexin (monoclonal mouse, 1:1000; Invitrogen, Carlsbad, California, USA), antiperipherin (polyclonal rabbit, 1:200; Millipore, Billerica, Massachusetts, USA), anti-CD68 (monoclonal mouse, 1:200; Dako, Glostrup, Denmark), antiphosphorylated neurofilament (pNF, monoclonal mouse, 1:600; Dako, Glostrup, Denmark) and parvalbumin (polyclonal mouse, 1:1000; Sigma Aldrich, St Louis, Missouri, USA). Diaminobenzidine (Wako, Osaka, Japan) was used as the chromogen.

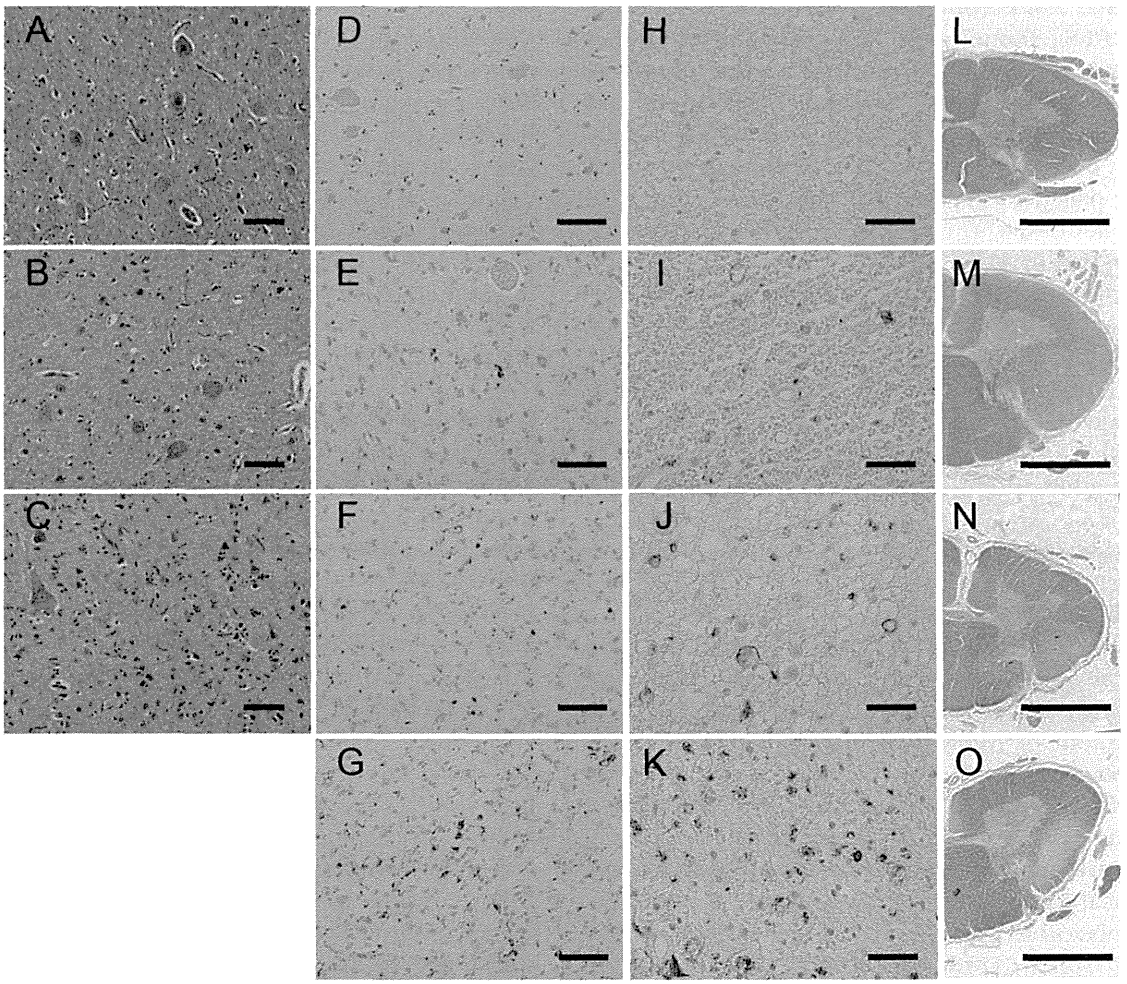

Figure 1 Measures of degeneration in the upper motor neuron system. (A–D) Loss of Betz cells in the primary motor cortex: stage (−), the Betz cells were spared in number and gliosis was absent (A); stage (+), mild neuronophagia and gliosis were noted (B) and stage (++), marked neuronophagia and glial proliferation were observed (C). (D–K) Aggregation of CD68 macrophages in the primary motor cortex (D–G) and the corticospinal tract in the lateral column of the spinal cord (H–K): stage (−), the aggregates were absent (D and H); stage (+), the aggregates were occasionally present (E and I); stage (++), the aggregates were present at a number of 1–5/ ×100 field (F and J) and stage (+++), the aggregates were diffusely observed (G and K). (L–O) Myelin pallor in the corticospinal tracts (CST) of the lateral column of the spinal cord: stage (−), myelin pallor was not detected (L); stage (+), myelin pallor was slightly notable (M); stage (++), myelin pallor was moderate (N) and stage (+++), the CST was entirely pale. (A–C) H&E staining, (D–K) anti-CD68 immunohistochemistry and (L–O) Klüver-Barrera staining. Scale bars: (A–G) 100 μm, (H–K) 50 μm and (L–O) 3 mm.